Final work : Design of the first stage of a centrifugal compressor with R1234ze(E) for heat pump in district heating

Auteur : Fois, Antonio
Promoteur(s) : Hillewaert, Koen
Faculté : Faculté des Sciences appliquées
Diplôme : Master en ingénieur civil en aérospatiale, à finalité spécialisée en "turbomachinery aeromechanics (THRUST)"
Année académique : 2020-2021
URI/URL : http://hdl.handle.net/2268.2/13222

THRUST Master of Science,
Master Thesis Project Report, 30 CET,
Universitè de Liege - Faculty of Applied Sciences
Academic year 2020-2021

Design of the first stage of a centrifugal compressor with R1234ze(E) for heat pump in district heating

Final work carried out with a view to obtaining the master's degree ”Civil Engineer in Aerospace with specialization in turbomachinery aeromechanics” by Fois Antonio Sebastiano

Author

Antonio S. Fois (antonio.s.fois@gmail.com)
THRUST Master of Science Graduate student
Université de Liege, Liege, Belgium, Aero & Meca Department, 2020-2021
KTH Royal Institute of Technology, Stockholm, Sweden

Accademic Supervisors

Koen Hillewaert,
Professor and Researcher, Université de Liege, Liege, Belgium
Jens Fridh,
Professor and Researcher, KTH Royal Institute of Technology, Stockholm, Sweden
Yang Gao,
Post Doc researcher, KTH Royal Institute of Technology, Stockholm, Sweden

Abstract

District heating is expected to play a key role in the energy grid and supply, particularly when heat pumps are connected to the system, and could cover up to 50% of the heating demand in Europe with heat pumps delivering around 25% of the energy transported by the district heating grid. In particular, High Temperature Heat Pump (HTHP), i.e heat pumps with heat sink temperatures equal or greater than 100°C, are regarded as excellent solutions for the district heating when the used electricity is green and there is a growing market in that area. However, the mass-production of these technologies is hindered by factors such as lack of available refrigerants with low Global Worming Potential (GWP) in the high temperature range and the technical challenges related to the compression process at high temperatures. This work addresses one of the main challenges currently present in the heat pump industry: to increase the Coefficient of Performance (COP) of a high temperature heat pump with a temperature lift of 105°C through the coupling of the thermodynamic cycle and centrifugal compressor design. In particular, an alternative approach to the optimization of the cycle is presented, researching the pressure ratio of the first stage that delivers the highest COP possible for given evaporator and condensing temperatures. Once this optimum pressure ratio is selected, the 1D meanline design of the compressor is assessed, an iteration loop between these two steps is followed until the efficiency resulting from the 1D design matches the one used in the thermodynamic cycle. A 3D CFD simulation is then assessed and its results are compared with the results of the two previous phases. The results obtained are promising, showing a COP of 2.61 that is significantly higher compared to the ones of state-of-art heat pumps with similar temperature lifts. Moreover, the results between thermodynamic cycle, 1D meanline design and CFD simulations have shown a strong agreement in the parameters observed, namely mass flow rate $\dot{m}$, total inlet and outlet temperatures T_{01} and T_{02}, total-to-total pressure ratio Π_{tt} and isentropic efficiency η^{is}, with a maximum variance of 4.6 % showed for the mass flow obtained in CFD. Additionally, the compressor design also addresses another industry challenge, that is to deliver high efficiencies and wide operating range at the same time. The present work present a centrifugal compressor with a 80% efficiency and able to operate at mass flow in the range [115-85]% before choking and surge.

Keywords

District heating; High Temperature Heat Pumps; Centrifugal Compressor Design; Coefficient of Performance; 1D Meanline Design; CFD

To the memory of my Grandfathers Antonio and Sebastiano, my greatest role models.

Acknowledgements

I would like to express my gratitude to all the people who helped me in this important achievement of mine.

First of all, I would like to thank the THRUST programme commitee, Nenad Glodic, Rober Kielb and Ludovic Noels, for having taken a chance on me, the biggest of my life until now. To professor Jens Fridh for all willingness to help demonstrated in the last two years, ultimately supervising me in this master thesis project. To Yang Gao, for guiding me through the completion of this master thesis, all the patience and empathy demonstrated in this last semester are greatly acknowledged.

To my professor Koen Hillewaert, for his kind help and for the passion for turbomachinery he transmits to us every day.

To the fantastic THRUSTERS, Akshay, Bart, Elena, Suzanne, Matias, Yash, Rupak and Lino, we are a small but amazing group and I look forward to meet you all again soon. A special thanks to my Indian brother Akshay, these two years would have never been the same without you, I wish to you all the luck of the world for your future and I am sure one day we will be partners, so be ready.

To the amazing people met in these two years both in KTH and ULg: Kay, Miguel, Xavi, Alex, Pol, Pietro, Giulio, Rosa, Sofia, Clemence, Leoni, Diogo, Mariana and everybody else who contributed to make all this time so crazy and beautiful. Special thanks to my homie Lollo Cantoni, for the laughs in every single moment of those months in KTH and for the amazing talks.

Most of all, extremely thankful to my family and friends back home. First of all to my mother Vittoria, who has always encouraged, supported and believed in me when few others did, her love and trust are what ultimately fueled my ambitions as kid and my efforts as a man. To my father Pietro, for the right words at the right time, when they most mattered, and whose work and sacrifice gave me the chances to become who I wanted to be. To my lovely sisters Maria Clotilde and Marianna, for being so perfect with such a bad brother. You are my best friends and there is no other people I rather spend more time with than you, together we are the best trio ever. To my uncle Pietro Paolo, my life mentor, for his willingness to help, his attention and invaluable pieces of advice. To my aunt Linda, for her always encouraging words and the help in fixing

my really bad English. Last, but not least, to my aunt Antonella and my grandmother Maria Clotilde, for the unconditional love they demonstrate every day to me and my sisters.

I need to thank my friends from home: Nicola, Pier, Anto & Riki Puddu, Gigio, Rikuz, Bifu, Mikkela, Tiziana, Massimo, Ial, all the AGVZZZ group and most of all to Sergio, home is wherever I am with you guys. To my partner in crime Tina and all the Presi Bene (PB) gang, you people are crazy and you totally saved my last four months.

To my friends from PoliMi: Fabio, Giovanni, Diego, Giulio, Leo, Asso, Ivo, Nich, Notar and the other countless people of those amazing years, for the incredible time we had in Milan, PoliMi was a bit more enjoyable with you on my side and I learned something from each of you. Giulio, you saved my life.

Finally, I need to thank Beatrice, you have been my trailblazer for years and an important fellow-traveller in the journey that ultimately led me until here, so this achievement is also yours.

Nomenclature

Acronyms

HTHP	High Temperature Heat Pump
GWP	Global Worming Potential
CC	Centrifugal Compressor
CFD	Computational Fluid Dynamics
IEA	International Energy Agency
HPT TCP	Technology Collaboration Programme on Heat Pumping Technologies
HP	Heat Pump
COP	Coefficient of Performance
RANS	Reynolds Averaged Navier–Stoke

Contents

1 Introduction **1**
1.1 Problem Statement & Objectives 2

2 Theoretical Background & State-of-the-Art **4**
2.1 Heat Pumps 5
2.2 Centrifugal Compressors Design 9
2.2.1 Kenematic parameters 15
2.2.2 Thermodynamics and Gas properties 17
2.2.3 Geometric parameters 17

3 Methodology **20**
3.1 Heat Pump Thermodynamic cycle 20
3.2 Mean-line design of the compressor 22
3.2.1 Duty and Aerodynamic Data 23
3.2.2 Gas properties 24
3.2.3 Geometry 25
3.3 3D design and CFD 27

4 Results & Discussion **32**
4.1 Heat Pump Thermodynamic cycle 32
4.2 Mean-line design of the compressor 35
4.3 3D design and CFD 37

5 Conclusions **40**

Chapter 1

Introduction

District heating is expected to play a key role in the energy grid and supply, particularly when heat pumps are connected to the system, and could cover up to 50% of the heating demand in Europe with heat pumps delivering around 25% of the energy transported by the district heating grid [1]. In particular, HTHP, i.e heat pumps with heat sink temperatures equal or greater than 100°C, are regarded as excellent solutions for the district heating when the used electricity is green and there is a growing market in that area. However, the mass-production of these technologies is hindered by factors such as lack of available refrigerants with low GWP in the high temperature range and the technical challenges related to the compression process at high temperatures.

Currently, R134a is the refrigerant commonly in use in heat pumps for district heating and presents a GWP around 1430. However, low global warming potential refrigerants, such as R1234ze(E) with GWP ~ 6, are anticipated to be the refrigerants of choice for high temperature heat pump systems in industrial applications. Moreover, the Centrifugal Compressor (CC) technology is seen as an attractive option compared with positive displacement compressors, since it presents key advantages such as the potential for high efficiency together the possibility to operate at high pressure ratios, still maintaining a compact design [2].

The present master thesis project is a joint collaboration between Siemens Energy AB ® and the Energy Department at KTH Royal Institute of Technology, the projects explores the design of the first stage of a centrifugal compressor with R1234ze(E) for a HTHP with a temperature lift of about $105°C$.

The work is structured as follows: Chapter 1 presents a first introductory overview on the field of heat pumps additionally to the problem statements and objectives. In Chapter 2, the theoretical background and state-of-the-art about heat pumps systems and thermodynamic cycle together with centrifugal compressor design are discussed. The methodologies followed in the project will be exposed in Chapter 3 while Chapter 4 will present and discuss the results obtained. Finally, the conclusions and future work will be exposed in Chapter 5.

1.1 Problem Statement & Objectives

The main challenge one can face while designing a Heat Pump is the interdependence between the thermodynamic cycle and the design of the compressor, the thermodynamic aspects of the cycle influence the fluid dynamics aspects of the compressor design and vice-versa and the process required to arrive at a final compressor design can be long and require a high number of iterations between every step. A general flow of the design work would be as follow:

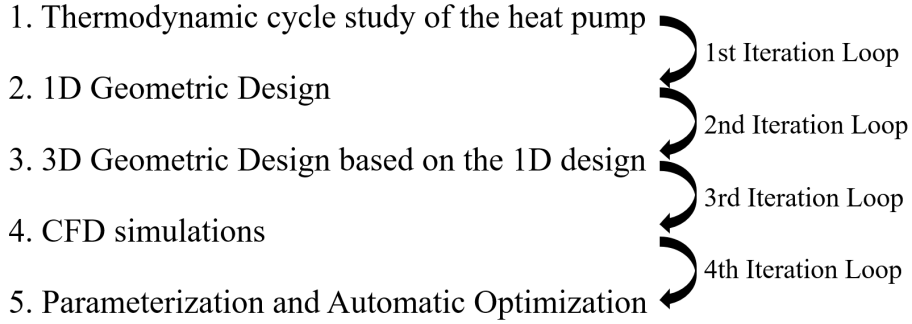

As previously anticipated, the present master thesis was carried on inside a broad project of Siemens Energy AB about heat pumps for district heating, however, the objectives and specifics requirements presented in this work should only be considered as general industry's goals and not related to any particular product development. The initial project description and problem statement as presented by Siemens Energy was the following:

In the project the one of the main goals is to design a compressor which can handle about $-5°C$ *evaporator temperature and about* $100°C$ *condensing temperature. The project explores the selection of refrigerant, cycle study and implementation of refrigerant/s in numerical tool and the flow simulation/evaluation of the centrifugal compressor in CFD. The compressor should be 2 stages centrifugal compressor. The compressor design can be a generic one and should be scalable. Two master thesis students are expected to perform the thesis: one thesis focuses on the heat pump process while the the other one makes a compressor aerodesign.*

As clear, the present project was initially designed for two students, one exploring the selection of refrigerant, cycle study and implementation of refrigerant/s in numerical tools while the second one designing the centrifugal compressor with meanline and CFD methods. The two students should have collaborated in order to deliver an optimum design. However, it was possible to find only one of the two students, i.e. the author of this thesis. As a consequence, the objectives of the master thesis project were re-calibrated, finally resulting in:

Design of the fist stage of a centrifugal compressor for a heat pump which can handle about $-5°C$ *evaporator temperature and about* $100°C$ *condensing temperature. The project must explore the cycle study and implementation of refrigerant in numerical tool and the flow simulation/evaluation of the centrifugal compressor in CFD. The compressor should be 2 stages centrifugal compressor. The compressor design can be a generic one and should be scalable.*

The key outcomes of the work hence resulted in:

1. Assessment of the thermodynamic cycle with the creation of a Matlab code able to run with every refrigerant in the CoolProp library. For a selected refrigerant the optimal pressure ratio for first and second stage of the compressor are selected, these are the pressure ratio delivering the highest coefficient of performance (COP) of the full heat pump cycle. The reference refrigerant used was R1234ze(E)
2. Design of the first stage of the compressor based on the inputs coming from the thermodynamic cycle, comprehensive of:
    - 1-D mean-line design using VISTA CCD and parametrical optimization using the Direct Optimization module in Ansys WorkBench
    - 3D design and CFD simulations using BladeGen, Turbogrid and CFX, respectively for the geometry, mesh, and CFD parts, in Ansys WorkBench

Chapter 2

Theoretical Background & State-of-the-Art

As could be already grasped, the present project combines the heat pumps thermodynamic cycle with centrifugal compressor design. In this section a mixture of theoretical background and state-of-the-art regarding this two technologies will be presented.

In the design of a Heat Pump (HP), it is of common practice to decouple the design of the thermodynamic cycle from that of the compressor, examples of this approach are found in previous studies such as Domanski et al. [3], McLinden et al. [4] and Kondou et al. [5]. However, decoupling these two processes may lead to inaccurate estimations of the thermodynamic cycle performance on the one hand, while complex or unfeasible compressor designs on the other hand. Moreover, although in this case the refrigerant was selected a priori, this could add an additional degree of freedom to be considered, as it could affect both the cycle and the compressor. In the recent years, some examples of combined design of the system and turbomachine in HP designs made their appearance in literature, among these the most relevant are the works from Shiffmann [6], Shiffmann & Favrat [7] and Javed et al. [8], which all proposed methods for coupling CCs designs with heat pumps cycles in different operating conditions. Meroni et al. [2] combined the design of a turbomcompressor and the heat pumps system additionally including the selection of the most suitable refrigerant. However, it should be noted that in all the previously cited works the design of the compressor stops at the 1D mean-line design. Other works, such the ones from Eckert et al. [9] and [10] involved both the 1D design and 3D CFD simulations, but do not consider the thermodynamic cycle in the design process. In the present work, a thermodynamic cycle study was firstly assessed where the optimum pressure ratios, i.e. the one delivering the maximum COP of the cycle, for the first and second stage were identified. Secondly, a 1D mean-line design of the two stages were implemented and optimized through a parameterization process. Finally, the 3D CFD simulations were assessed, considerably increasing the computational time and efforts. In the author's knowledge, very few works describe so in detail the full design process of a centrifugal

compressor for heat pumps, starting from the thermodynamic cycle and concluding with the 3D CFD simulations, and he is not aware of any among these works that focused on heat pumps with temperature of 100° C or above.

2.1 Heat Pumps

Heat pumps have evolved to become a mature technology over the past two decades, since they offer efficient means to reduce primary energy consumption by utilizing heat recovery they are regarded as a viable and attractive solution to look forward to the enhancement of energy efficiency and savings ([11], [12]). The International Energy Agency (IEA) have been putting efforts in the research about these technologies since 1978 through the Technology Collaboration Programme on Heat Pumping Technologies (HPT TCP), which counts 17 member countries. One of the main activities within the HPT TCP is to run collaborative research, development, demonstration and deployment projects, called Annexes. As reported in the Annex 47 [13] of IEA, heat pumps can become key technologies particularly in district heating grid, for many reasons: they can balance the grid when the electrical production from intermittent renewable energy sources fluctuates; using low and ultra-low temperatures they can reduce the grid losses; they can increase the flexibility of district heating systems by expanding the heat generation portfolio, eventually bringing economical advantages; they augment the renewable heat generation ultimately helping to phase out fossil fuels from the energy system.

The application of heat pump systems is currently extending to the generation of high-temperature heat pumps. Although its definition is not consistent in literature, the term high-temperature heat pump is generally referred to a heat pump with sink temperature in the range 100–150 °C. The present work assumes, in agreement with other authors such as Meroni et al. [2], 100°C as the boundary for classifying a HTHP. The HPT TCP by IEA is currently working, among other projects, on the Annex 58, specifically focused on HTHPs. The objective of the annex is to provide an overview of the technological possibilities and applications as well as to develop concepts and strategies for the transition towards heat pump-based process heat supply, aiming to improve the understanding of the technology's potential among various stakeholders, such as manufacturers, potential end-users, consultants, energy planners and policy makers. The final report of Annex 58 is expected to be published late 2023.

Chua et al. [14] reviewed the heat pumps practical solutions known until 2010, already anticipating that the development of better compressor technology had the potential to reduce the energy consumption by 80%. Zhang et al. [15] reviewed the research work done and the advances in the application of industrial heat pump systems in China, including advances in the refrigerants, multistage systems, double-effect absorption systems, compression-absorption, solar assisted system and chemical heat pumps. Van de Bor & Ferreira [16] presented a method to quickly select the most suitable heat pump type, depending on economic and performance requirements, based on the lift to sink temperature ratio for the process fluids, although the

proposed method is more widely applicable the study focuses on the application of heat pumps at distillation columns. It was also shown that, for mechanical heat pumps, making use of the available temperature glide increases performance and reduces the payback period. While at low glides heat driven absorption heat pumps and vapor (re)compression heat pumps show the smallest payback times, mechanical heat pumps with large glides show to be more effective at higher temperature lifts when temperature glides are available. Due to improved performance, these mechanical heat pumps are able to achieve better economical results over their technical life time although they require higher initial investment.

Regarding HTHPs, Arpagaus et al. [17] in 2018 published a comprehensive review of the most important advances in the field, with a market overview, research status, theoretical background of the thermodynamic cycles, system performance and an additional focus on the selection of refrigerants. In Arpagaus's work, 20 HTHPs from 13 different manufacturers were identified among those able to deliver heat sink temperatures higher than 90°C. These machines were both single-staged and two stages, with temperature lifts between 30°C and 70°C and operating with refrigerants such as R245fa, R717, R744 as well as R1234ze(E).

Heat pump is a very broad subject and it is therefore impossible to be fully addressed in the context of this master thesis, which rather focus on the interplay between thermodynamic cycle and centrifugal compressor design. However, it will be here provided an overview of its theoretical background. A heat pump is defined as a device that moves (or 'pumps') thermal energy opposite to the direction of spontaneous heat flow by absorbing heat from a cold source at a temperature T_C, also called sink temperature, and releasing it to a warmer one at at temperature T_H, also called source temperature. The difference between the sink and source temperature is defined as temperature lift $T_{Lift} = T_H - T_C$.

In general, heat pumps can be divided in 3 types [16]: mechanically driven, heat driven and heat transformers. Among these three categories, the major types of industrial heat pumps are [18]:

- Closed vapor compression heat pumps (VCHP)
- Vapor recompression cycles
- Absorption heat pumps

Mechanically driven closed vapor compression heat pumps are the most widely used and available in a large variety of sizes for different applications [19], these systems transfer heat through a closed-loop cycle by compressing, condensing, expanding, and evaporating a refrigerant fluid. In the simplest configuration a heat pump indeed consists of an outdoor unit, comprehensive of a compressor and a heat exchanger working as an evaporator in winter and a condenser in summer, and an indoor unit with another heat exchanger complementary to the previous one (condenser in winter and evaporator in summer). However, in the present project only the winter configuration was considered. Figure 2.1.1 show the schematic diagram and T-s

diagram of a generic one stage heat pump.

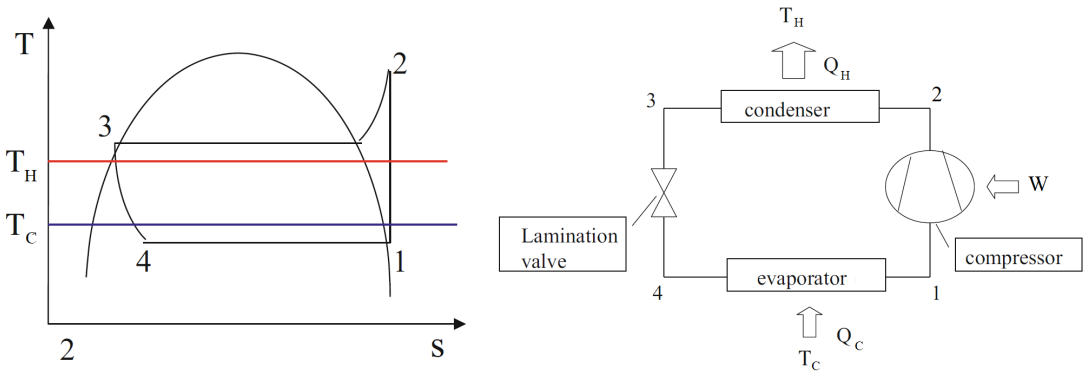

Figure 2.1.1: One-staged heat pumps system schematic diagram (left); T-s diagram as represented by [20]

Generally, one can apply the first and second principles of thermodynamics (Eq. 2.1 and 2.2 respectively) as follows:

$$Q_H + Q_C = W; (Q_H < 0; W < 0) \tag{2.1}$$

$$\frac{Q_H}{T_H} + \frac{Q_C}{T_C} + S_g = 0 \tag{2.2}$$

where H and C respectively indicate the hot and cold sources, Q is the heat exchanged with thermal sources, W is the work supplied to the system, T their thermodynamic temperature and S_g the amount of produced entropy. Now, rearranging and substituting Eq. 2.2 into Eq. 2.1, one can get to the definition of Coefficient of Performance (COP), a coefficient that characterizes heat pumps performances as the ratio of heat exchanged with indoor environment and the mechanical work supplied to the machine. This is positive by definition and for the winter configuration of the heat pump is given by the following relation:

$$COP = \frac{Q_H}{W} = \frac{1}{1 - \frac{Q_C}{|Q_H|}} = \frac{1}{1 - \frac{T_C}{T_H}\left(1 - \frac{T_H S_g}{|Q_H|}\right)} \tag{2.3}$$

Beside the specific requirements of this project, it is generally more efficient to split the compression transformation in two or more stages when great pressure ratios need to be achieved, in the case of heat pumps the pressure ratio is mainly due to the temperature lift, Mateu-Royo et al. [21] have shown that two-stage cascade becomes the most appropriate configuration for temperature lifts of 60 K and above. In the case of a two-stage closed vapour compression heat pump system, the working principle of is well described by Hu et al. [22]: the liquid refrigerant in the evaporator absorbs heat from the waste water and vaporizes, reaching the inlet of the first stage of the compressor (1), then the super-heated refrigerant vapour is compressed to an intermediate temperature and intermediate pressure gas by the first stage (2). At this point, the discharge gas from the first stage is mixed with the intermediate pressure vapour refrigerant

from the flash tank, reaching a intermediate point in (3). The mixed vapour successively enters the second-stage for the high-pressure compression, from the outlet of the second stage the refrigerant flows into the condenser where it exchanges heat with the water from the water supply system and becomes liquid refrigerant (5). The water in the condenser is heated up after absorbing heat from the refrigerant gas and circulates back to the water supply system while the saturated liquid refrigerant pass through the subcooler where it is further cooled down until point (6). The high pressure refrigerant from the subcooler is then throttled by the upper-stage expansion valve and becomes a liquid-gas mixture of intermediate pressure. From here (7), the refrigerant mixture is then separated into liquid phase and vapour phase in the flash tank with intermediate pressure. The liquid refrigerant is further throttled by the first stage expansion valve and becomes a liquid-gas mixture of low pressure and low temperature (9). The vapour refrigerant of intermediate pressure is mixed with the discharge gas from the first stage compression (8) and repeats upper cycle previously described. Finally, the low pressure refrigerant mixture in (10) flows back to the evaporator where it absorbs heat from waste water and vaporizes until it reaches again (1), ready for the next cycle. The process previously described is represented in Figure 2.1.2 below with the system schematic, P-h and T-s diagram:

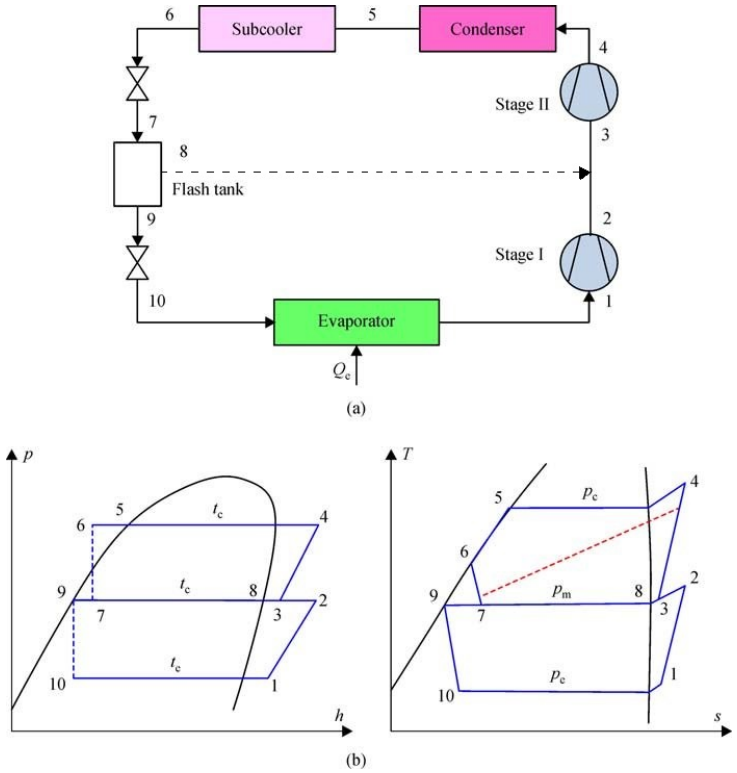

Figure 2.1.2: Description of two-stage compression heat pump system (a) Schematic diagram; (b) diagrams of p-h and T-s as represented by [23]

The super-heating control applied before the compressor inlet is mainly required to prevent wet fluid compression and consequent compressor damage [24], the minimum super-heat depends on the refrigerant, the condensation and evaporation temperatures and the isentropic compressor

efficiency, but it can vary between 0 and 35 K [25]. In the present project, the minimum super-heat for fixed sink and source temperature was selected as the super-heat necessary to avoid cutting the saturation curve during compression, as it will be explained in Chapter 3.

In the case of a two-stage heat pump, one can hence apply a similar reasoning as for the single stage and obtain the following expression for the COP:

$$COP = \frac{Q_H}{W} = \frac{m_2(h_4 - h_6)}{m_1(h_2 - h_1) + m_2(h_4 - h_3)} \tag{2.4}$$

where m_1 and m_2 represents the mass flow flowing respectively through the first and second stage, while h_i represent the entalpies of the refrigerant at the state point i.

2.2 Centrifugal Compressors Design

Turbomachines employing centrifugal effects (i.e. CCs) for increasing fluid pressure have been in use for more than a century and in a series of different fields such as aerospace, automotive, chemical, energy production and large-scale air conditioning. The progress of the technology in the last decades, such as the introduction of high-speed generators, have made it possible to apply CCs even to smaller units in the refrigeration and heat pump fields [2], making these technologies preferred to reciprocating and screw compressors since their higher initial cost is generally offset by improved energy efficiency [26]. Already in 1985, CCs were the choice for refrigerating plants and compression types used in district schemes [27].

A centrifugal compressor essentially consists of a rotating impeller, generally composed by an alternation of blades and splitters (half blades), followed by a diffuser. The purpose of the impeller is to increase the energy level of the fluid by whirling it in the outward direction, hence increasing the angular momentum of the fluid. Within the impeller, both static pressure and velocity are increased. Conversely, the function of the diffuser is to convert the kinetic energy of the fluid leaving the impeller into pressure energy, this can be accomplieshed by free diffusion in the annular space surrounding the impeller (i.e. vaneless diffuser) or through a row of fixed diffuser vanes (i.e. vaned diffuser) allowing a much smaller frontal area of the machine. In order to reduce the degree of complexity, consequently saving the time required for the design of the diffuser vanes, and not having specific requirements regarding the frontal area of the compressor in this project it was decided to implement a vaneless diffuser. Outside the diffuser generally is a collector scroll (or volute), since its function is primarily to collect the flow at the diffuser outlet and deliver it to the outlet pipe, hence not affecting drastically the overall thermodynamics, kinematics and performances of the compressor, it will not be considered inside the scope of the present work. Figures 2.2.1 show a generic impeller drawing while Figure 2.2.2 represents a meridional and frontal view of a vane-less centrifugal compressor stage. The hub of a turbomachinery is the surface of revolution to which the rotor blades are attached to, i.e. the curved surface *a-b* of Figure 2.2.2, while the shroud is the curved surface *c-d* forming

the external boundary of the fluid domain. At the inlet of the impeller, also called eye (section

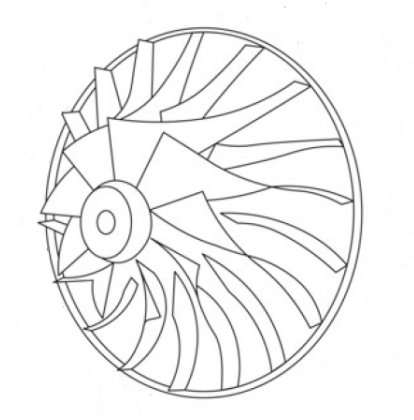

Figure 2.2.1: 3D representation of a centrifugal compressor impeller

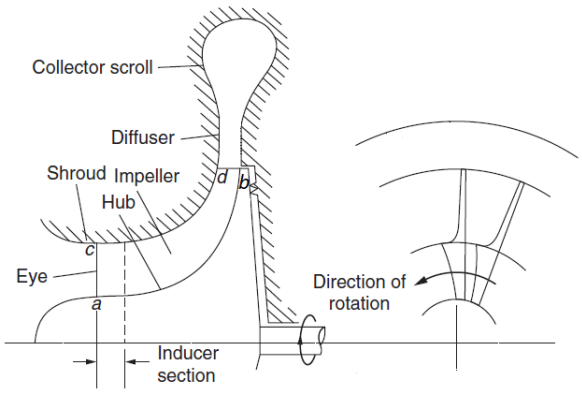

Figure 2.2.2: Centrifugal compressor sketch, meridional and frontal view

a-c), the absolute flow arrives with a velocity c_1 and an angle α_1 (commonly $\alpha_1 = 0$), while the relative flow has a velocity w_1 and an incidence angle β_1 with respect to the axis of rotation. The inducer, the region starting from the eye and generally terminating where the flow is beginning to turn into the radial direction, then deviates this relative flow towards the axial direction. At the outlet of the impeller, the absolute flow will leave the blades at a velocity c_2 and an inclination α_2. The general velocity triangles of a centrifugal compressor are presented in figure 2.2.3 below:

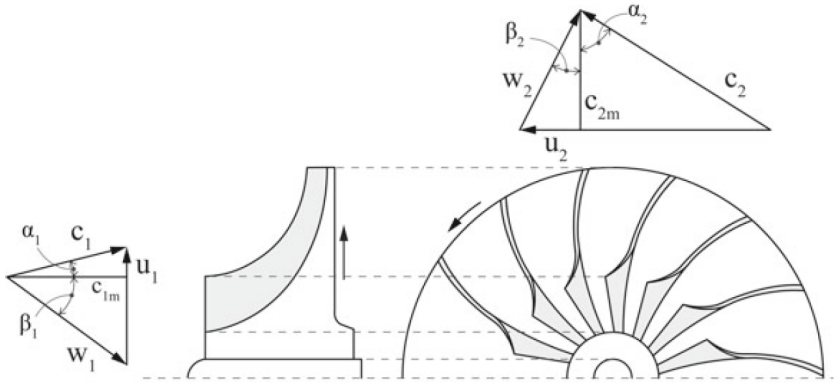

Figure 2.2.3: velocity triangles in a radial compressor stage

In can be observed that the flow inside a centrifugal compressor has components of the velocity in the radial, tangential and axial direction, respectively indicated as c_r and c_θ and c_x, hence the absolute velocity is given by $c^2 = c_r^2 + c_\theta^2 + c_x^2$. An important mechanical property, first introduced by Wu in 1952, is the rotational stagnition enthalpy, widely known as *rothalpy*, this can be obtained starting from the Euler work equation, Eq. 2.5, showed below:

$$\Delta h_0 = \Delta(U c_\theta) \tag{2.5}$$

where h_0 is the total enthalpy, c_θ the velocity in the tangential direction and U the blade speed, obtained as the product between the roational speed Ω, in rpm, and the radius of the impeller. Therefore, substituting the expression of the total enthalpy that relates it with the static enthpaly and the flow velocity $h_0 = h + (1/2)c^2$, one can rewrite Eq.2.5 as:

$$I = h + \frac{1}{2}c^2 - Uc_\theta \tag{2.6}$$

where h is the total enthalpy, c is the absolute flow velocity and I is the rothalpy, that is constant along the impeller. Now, substituting the definition of c into Eq. 2.6 one can obtain:

$$I = h + \frac{1}{2}(c_r^2 + c_\theta^2 + c_x^2 - 2Uc_\theta) \tag{2.7}$$

Subtracting $(1/2)U^2$ and substituting the expressions deriving from the velocity triangles $U - c_\theta = w_\theta$ and $w^2 = c_r^2 + w_\theta^2 + c_x^2$ one has:

$$I = h + \frac{1}{2}(w^2 - U^2) \tag{2.8}$$

Since across the impeller the rothalpy is constant, i.e. $I_1 = I_2$, one finally have:

$$h_2 - h_1 = \frac{1}{2}(U_2^2 - U_1^2) + \frac{1}{2}(w_1^2 - w_2^2) \tag{2.9}$$

where the pedix 1 and 2 represent the inlet and outlet of the impeller respectively. It comes now clear that the static enthalpy rise in a centrifugal compressor stage is significantly larger compared with a stage of an axial compressor, hence providing higher pressure ratios for a given number of stages, making these types of machine preferred when size is a constraint, such as in heat pumps for district heating. Indeed, while the second therm on the right hand side is also present in the case of axial compressors, the first term, $(1/2)(U_2^2 - U_1^2)$, is the contribution of the centrifugal action caused by the change in radius between the impeller inlet and outlet.

Applying the same reasoning inside the diffuser and remembering that in this region, since $U = 0$, the relative and absolute velocity coincide, one has:

$$h_3 - h_2 = \frac{1}{2}(c_3^2 - c_2^2) \tag{2.10}$$

The relations above presented can be traced in Figure 2.2.4.

A variety of books ([27], [28], [29], [30]) about turbomachinery design provide the general procedure followed for the development of the preliminary design of centrifugal compressors, i.e. the calculation of the kinematic, thermodynamic and geometric parameters as well as the stage losses, that are ultimately related to the efficiency of the compressor. As can be already grasped, the flow inside a centrifugal compressor stage is a highly complicated 3D motion, to have a first simplified evaluation of this flow it is of common practice in the design of centrifugal

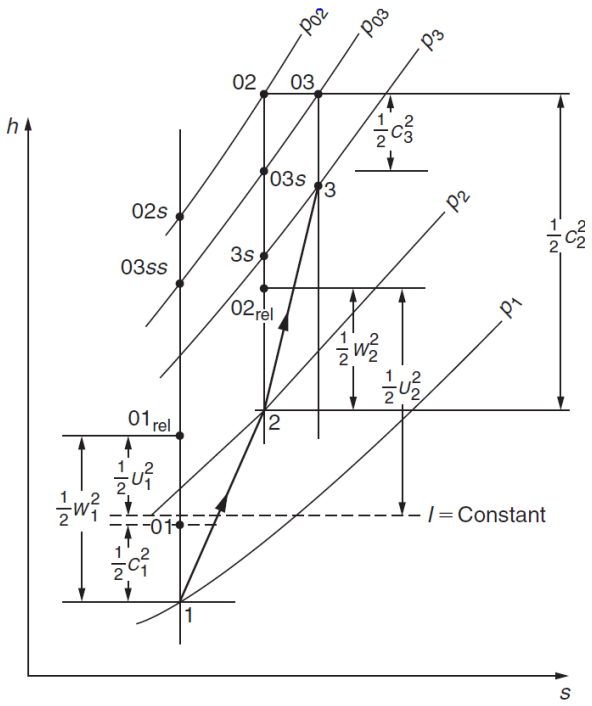

Figure 2.2.4: Mollier diagram for a centrifugal compressor stage (impeller and diffuser)

compressors to start with a 1D approach, also known as mean-line method, which assumes that the fluid conditions are uniform over a specific cross section of the flow, generally the mid-span. The 1D mean-line method can give approximate results in a relatively short time and with low computational effort compared to other advanced methods such as through-flow or Computational Fluid Dynamics (CFD), however these last two methods are obviously more accurate and is necessary to use them in the advanced phases of the design. 1D designs are generally achieved through numerical methods that provide the geometry (e.g. approximate blade shape, inlet and outlet heights, blade angles etc.) as well as the basic aerodynamics (e.g. velocity triangles) and the performance estimation of the compressor through the solution of the governing equations at the mid-span streamline and main stations of the compressor components (e.g. impeller inlet/outlet, diffuser inlet/outlet etc.).

Harley et al. [31], after having investigated different 1D methods for the performance prediction of CCs, concluded that the 1D single zone method is the most suitable for the preliminary design process, since it provides the opportunity to analyze and reduce the internal losses even for modern designs.

Inside 1D methods, many design strategies are in use for the design of compressors. Two of the initial parameters are generally the total temperature and pressure at compressor inlet, namely T_{01} and p_{01} but then different design strategies require different additional inputs. Some of these strategies may well start from the definition of non-dimensional coefficients such as the flow coefficient ϕ and the work coefficient ψ, with the addition of other parameters such as degree of reaction R or meridional velocity ratio ε, the tip Mach number M_u, the rotor tip diameter ratio σ_t, flow angle at inlet α_1 and the stage efficiency η. Other methodologies may, on the other side,

start from dimensional values such as rotational speed N and mass flow rate $\dot{m}$, plus the total-to-total pressure ratio of the compressor Π_c. In all cases it is however always possible to pass from dimensional parameters to the non-dimensional ones and viceversa. The main advantage of the non-dimensional parameters with respect of the dimensional ones is to allow an easier scaling of the machine. The general process followed in a 1D mean-line design process is summarized in the block diagram in Figure 2.2.5 below:

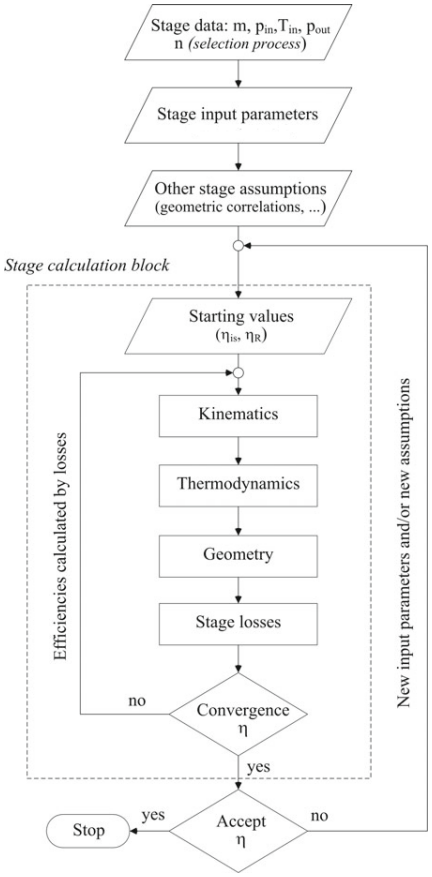

Figure 2.2.5: Block diagram for 1D mean-line design of a compressor stage [28]

As already said, the different parameters can be correlated between each other, for example the pressure ratio can be written in terms of the ratio of specific heats γ, work coefficient ψ, isentropic efficiency η_{is} and tip Mach number M_{u2} as follow:

$$\Pi = \left[1+\eta(\gamma-1)\psi M_{u2}^2\right]^{\frac{\gamma}{\gamma-1}} \tag{2.11}$$

where $\psi = \Delta h/U_2^2$ and $M_{u2} = U_2/\sqrt{\gamma RT_1}$. As shown by Robinson et al. [32] from PCA Engineers Limited (i.e. the developers of mean-line tool used in this project, VISTA CCD), the pressure ratio across the compressor, for a given refrigerant and inlet conditions, more or less fixes the Mach number at the tip as shown in Figure 2.2.6. Then, as per the relation used in VISTA CCD, the flow coefficient is related to the inlet volume flow $\dot{V}$, the diameter of the

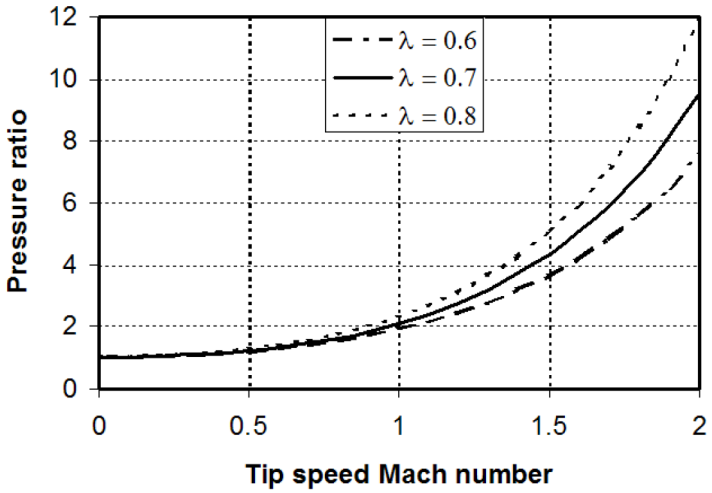

Figure 2.2.6: Influence of Mach number and work coefficient on pressure ratio

impeller outlet D_2 and the tip speed at impeller outlet U_2 as follows:

$$\phi = \frac{\dot{V}}{D_2^2 U_2} \tag{2.12}$$

Consequently, ϕ strongly affects the efficiency of the compressor and it also follow that, for a given pressure ratio, if the tip diameter is fixed then the shaft speed is also relatively constrained and vice versa. At a preliminary design phase, such in 1D mean-line design, it is of common practice to use empirical relations to correlate the performance of the compressor (i.e. the efficiency) with global parameters (e.g. ψ, M_{u2}), two well-known correlations of this type are the ones from Casey and Marty [33] and Rodgers [34]. These two correlations, the former related to tip speed Mach numbers up to 1 and the latter for higher Mach numbers, where then merged into a single one with the general form:

$$\eta = f(\phi, M_{u2}) \tag{2.13}$$

which finds graphical representation in Figure 2.2.7.

It can be observed that the highest efficiencies are generally obtained for flow coefficients in the range $0.06 < \phi < 0.09$, therefore it is of main interest for the designer of the compressor, and therefore also for the scope of this project, to select his decision variables to fall into this range. The specific parameters used, their effect on the compressor design and the range of their values selected in the present work will be better described in Chapter 3.

While CFD codes are rather difficult to implement, and hence it is generally preferable to rely on the main stable and accurate ones such as ANSYS CFX and Fluent or the open source OpenFOAM, it is more common to develop in-house mean-line codes, that can be more easily constructed based on a particular know-how and shaped in order to meet the specific requirements of an investigation. At the same time, the validity of each preliminary design

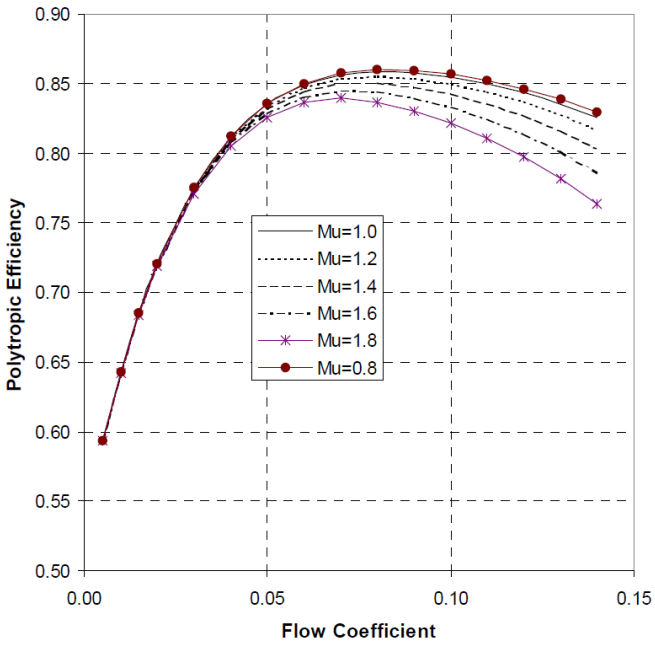

Figure 2.2.7: Casey-Robinson correlation as shown by the same authors in [32]

model has to be ensured in order to meet the accuracy and reliability criteria required in the design process of CCs. Meroni et al. [2] summarized the main mean-line models and their validation methods developed since 1956 to 2015.

As seen above, the main parameters in a compressor design can be divided in three main categories, namely kinematics, thermodynamics and geometry parameters. The main parameters of each category with their most used common practices and well-known effects on the design will be presented below:

2.2.1 Kenematic parameters

Amongst the aerodyanmic or kinematic parameters one can identify:

Mass flow rate $\dot{m}$: the mass flow rate has an influence on the blade height (once the impeller hub radius is fixed), these two together affects the blade thickness. Typical values of mass flows for turbocharger applications range from a few kilograms per seconds to over a hundred kilogram per second.

Rotational speed N: the rotational speed (rpm) is directly related to the tip diameter and speed at impeller outlet. Depending on the specific application and design, it can vary between 1000 rpm and 40.000 rpm, but some extreme cases can reach up to 200.000 rpm.

Relative velocity ratio W_2/W_1: the relative velocity ratio (or diffusion ratio) has a direct impact on the performance of the compressor, influencing the stall point, and on the geometry, affecting the blade width at exit. The major impact of the impeller blade exit width are on the flow capacity and the pressure ratio of the stage [35]. Depending on the design philosophies, many different

ranges of the diffusion ratio are proposed in literature, the overall lower and upper boundaries of these range were found to be 0.25 and 0.85 respectively.

Inlet flow angle at mid span α_{1m}: is not uncommon to set the impeller incidence at mid span at zero in order to reduce the relative Mach number at the impeller inlet.

Meridional velocity gradient at impeller inlet dc_m/dq: meridional velocity generally slightly increases from hub to shroud, however there no a general range of values for this parameter.

Choke ratio m/m_{choke}: the choke ratio defines the relationship between the mass flow rate at design point and the mass flow rate at choke point, obviously the first one cannot be grater than the second, i.e. the ratio must be lower than one. The stall and choke mass flow determine the operating range of the compressor, so this is an important parameter to be selected. Wang et al. [36] have shown that, for low flow coefficients centrifugal compressors, the highest efficiencies and pressure ratios are obtained for m/m_{choke} in the range 0.8–0.9, while when approaching 1 these two quantities decrease abruptly. In general, experience have shown that this range is reasonable also for machines with higher flow coefficients.

Flow coefficient ϕ: the flow coefficient is one of the most important characteristic parameters in centrifugal compressors and with the far reaching applications. It determines how great an actual volume flow is achieved by an impeller of a given diameter rotating at a given tip speed and it strongly affects the efficiency of the stage. Centrifugal compressors generally have a ϕ that can range from 0.007 to 0.02 for very low flow coefficients to more than 0.15 for high flow coefficients. Small ϕ implies narrow inlets and exit widths, losses generally tends to increase tending to the lower boundary, hence decreasing the stage efficiency and head, while the lower limit is dictated by the size and the increase of the impeller stresses [37]. In order to maximize the efficiencies and contain the losses and the size, a medium flow coefficient in the range 0.03-0.09 is desirable.

Work coefficient ψ: the work coefficient of a centrifugal compressor stage, defined as the ratio between the enthalpy change through the stage and the square of the rotational speed, is determined with the geometry of the impeller and kinematic of the flow, and with the gas dynamic efficiency. This coefficient is connected with the effective compression work and have a direct link with the pressure ratio of the compressor [38].

Blade mach number at impeller exit M_u: the blade mach number at impeller exit (or peripheral mach number) is the ratio between the blade speed at impeller outlet and the speed of sound at inlet. Sarevski [39] presented comparative of centrifugal compressors' stage data for some refrigerants with large molecular mass, hence similar to the present research, and showed that for similar tip speeds and size of the stage M_u can reach up to 1.6, although other cases can reach up to 2.

Tip speed at impeller outlet u_2: the limitation tip speed at impeller outlet is mainly given by the

corresponding peripheral mach number and loads, i.e. by the material used for the manufacture, that in the present case should be lower than 250 m/s.

2.2.2 Thermodynamics and Gas properties

The thermodynamics and gas properties depends on the thermodynamic cycle and refrigerant used. The gas properties can affect both the kinematic and geometric parameters, such as the Mach number or the sections area trough-out the machine, they can be assumed ideal in order to reduce the degree of complexity of the design, assuming average properties throughout the compressor stage, in this case the average gas constant R and specific heats ratio γ plus the inlet total temperature and pressure are the required parameters. It will be better explained in Chapter 3 that for heat pumps with very high temperature lifts and operating at condensing temperature close to the critical point of the refrigerant the real gas model is more appropriate, this model require additional parameters such as the polynomial coefficients of the function relating the specific heat at constant pressure c_p with the temperature together with other parameters, hence adding more complexity to the simulation environment, increasing the simulation time and introducing possible source of errors.

2.2.3 Geometric parameters

The most important geometric parameters that a designer should understand are presented as follow:

Backsweep angle β: the backsweep is probably the most important geometrical parameter since determines the shape of the impeller and of the compressor, as well as the flow characteristics, efficiency and performance characteristics of the centrifugal compressor (Sarevski [39]). In fact, the backsweep angle at impeller outlet β_2 directly affects the velocity triangle at impeller exit, when backweep is introduced this results in a steeper slope of the head-flow curve compared to the pure radial impeller exit, a steeper characteristic generally leads to improved flow range and more stable operation. However, on the other side backsweep has a great impact on the compressor efficiency and experience show that the efficiency is lower for higher values of β_2. The value of the backsweep angle needs therefore to be selected carefully and in a reasonable range.

Rake angle χ: the rake angle is the angle between the blade generatrix and a meridional surface. The rake angle values along the meridional coordinate are function of the meridional shape and the blade shape of the specific design. The value of the blade angle at the impeller trailing edge χ_2 defines the rake angles along the entire blade surface. A negative rake angle reduces the velocity gradient and create a more uniform flow, that can be considered a positive factor. However, a non-zero rake angle increases the blade surface, hence increasing the friction losses, while the blade blockade is smaller, that is a negative effect too. Arunachalam et al. [40] investigated the effect of rake angle on high-pressure aviation centrifugal compressors, showing

that high positive rake angles provide high efficiency, while high negative rake angles provide larger stall margin. Drozdov and Galerkin [41], suggested that a reasonable range for the rake angle at trailing edge would be between -30 and $+30$ degrees.

Number of blades and splitters Z_b: the number of blades and splitters can be derived in several ways. In general, experience have shown that the blade number is function of the total-to-total stage pressure ratio. Meroni et. al [2] and Xu and Amano [35] have proposed an empirical correlation which provides the number of blades (with or without splitters) on the base of the target pressure ratio.

Impeller outlet radius D_2: the impeller outlet radius is mainly limited by the target compressor size or specific size requirements imposed by the particular application. The value of D_2 have a direct impact on the tip speed velocity at outlet, hence affecting important parameters such as ψ.

Once the meanline is completed, 3D design and CFD simulations must be assessed to validate the 1D model and increase the degree of fidelity of the design to reality. CFD has been used in turbomachinery since late '70s by some of the main exponents in the field, such as Japikse [42]. Nowadays, CFD plays a central role in turbomachinery design and in literature a great variety of papers can be found regarding the CFD of centrifugal compressors. Saha et al. [43] reviewed the state-of-the-art of the CFD of centrifugal pumps, giving a broad overview on the topic. Dewar et al. [44] recently presented a CFD modeling for centrifugal compressor and validate it with experimental setup, stating that the two results have a discrepancy around one or two percent at design point, and can increase up to 5% moving away from it.

In general, the CFD simulations inside a compressor are based on the solution of the Reynolds Averaged Navier–Stoke (RANS) equations: Continuity Equation (conservation of mass), Newton's Second Law (conservation of momentum) and the First Law of Thermodynamics (conservation of energy). The proper set-up of the simulation domain will allow the correct resolution of this equations, i.e. the calculation of spatial changes of all physical properties for both fluid flow and heat transfer. There are different ways of modelling the CFD of a centrifugal compressor. The simplest level of approximation is to model only one single flow passage of the impeller and utilize a rotating coordinate system, this can be treated as a steady-state problem. Consequently, moderate computational effort is required, but the variation in boundary conditions that takes places during the rotational cycle are not considered. The second level of approximation is to model also stationary parts such as the inlet flow channel and the diffuser, in this approach the impeller is modelled in a rotating coordinate system, while the rest is stationary. In this case, it is not possible to render the computational problem steady by choosing a calculation domain that rotates with the impeller. The CFD programs offer different approaches for treating this problem, all of them are using multiple interfaces initially proposed by Tamma et al. [45] in 1999, these are namely the stage (or mixing plane) model, the frozen rotor model and periodic interface model. With the mixing plane interface quantities are averaged circumferentially at the interface while with the frozen rotor method pressure and

velocity are transferred directly across the interface, with the circumferential velocity adjusted by the local blade speed, the periodic interfaces are only used on the boundaries between circumferential sectors that are axis symmetric. The simulation domain is discretized in a number of small elements or cells, generating a mesh (or grid), these elements are used by the CFD solver to construct control volumes. Each cell of the mesh represents an individual solution of the RANS equations which, when combined for the whole network, results in a solution for the entire mesh. The shapes of control volumes depend on the capabilities of the solver. Structured-grid codes use quadrilaterals in 2D and hexahedrons in 3D flows. Unstructured-grid solvers often use triangles (2D) or tetrahedron (3D), but newer codes can use arbitrary polyhedrons. The choice of the domain, mesh and interfaces configuration greatly affects the results of the CFD simulations. Also the turbulence model, i.e. the mathematical model used to predict the effects of turbulence, play an important role, even though Rautaheimo et al. [46] indicated that the effect of the turbulence modeling, at least at the design point, is not of paramount importance. The most used turbulence models in CFD are mainly $k-\varepsilon$, $k-\omega$ and SST. K-epsilon [47] is the most common model used CFD to simulate mean flow characteristics for turbulent flow conditions, is a two-equation model which gives a general description of turbulence by means of two transport equations. The original impetus for the K-epsilon model was to improve the mixing-length model, as well as to find an alternative to algebraically prescribing turbulent length scales in moderate to high complexity flows. K-omega [48] is a common two-equation turbulence model that is used as a closure for the Reynolds-averaged Navier–Stokes equations (RANS equations). The model attempts to predict turbulence by two partial differential equations for two variables, k and ω, with the first variable being the turbulence kinetic energy (k) while the second (ω) is the specific rate of dissipation (of the turbulence kinetic energy k into internal thermal energy). SST combines the two previous methods using $k-\omega$ in the inner region of the boundary layer and switches to the $k-\epsilon$ in the free shear flow. K-omega model is very suitable for fully turbulent non-separated flows, but does not calculate very accurate flow field that exhibit adverse pressure gradient and strong curvature, such as the ones in centrifugal compressors. Problems related to external body can be simulated more accurately with $\mathrm{k}-\varepsilon$ model. Pecnik and Rinaldi [49] have recommended k-ω shear stress model (SST) for accurate simulation in near wall treatment and internal flow like turbomachinery. Finally, proper converge of the simulations must be assured and hence convergence criteria have been developed and sharpened in time, the recent study from Ameli et al. [50] offers a good spark for the proper selection of convergence criteria.

Chapter 3

Methodology

Looking at the broad overview about heat pumps and compressor design given in Chapter 2 it comes clear that the compressor design is strongly dependent on the thermodynamic cycle design and vice versa, although these two are often uncoupled in common practice. However, a coupling between basic compressor design evaluation and thermodynamic cycle calculations is required to obtain truly optimum design for a specific application, such as the one of a taylor-made high temperature heat pump for district heating. This chapter will present the methodology procedure followed in this project. Firstly, for a fixed refrigerant and temperature lift of the heat pump, the thermodynamic cycle was computed in order to obtain the boundary conditions of the compressors, such as target pressure ratio, efficiency and outlet temperature. Then, the 1D meanline design was developed and optimized. Finally, the 1D design was transformed into 3D and CFD simulations were assessed. The structure of this chapter reflects the process just described but it should be noted that the three different phases are strongly linked one to another and a number of back and forth iterations was needed to find the most suitable design. The different design phases and the methodology followed inside them are presented in the three sections below.

3.1 Heat Pump Thermodynamic cycle

The basic theory of heat pumps thermodynamic cycles was already presented in Chapter 2. In practice, there are several ways to compute the thermodynamic cycle, all of them require a real gas properties library and a programming language wrapper or high-level interface. The most used libraries are CoolProp [51] and REFPROP [52] and they are generally used inside the Engineering Equation Solver (EES) [53], MatLab [54] or Python [55]. In this project, the fluid properties were computed using real-gas equations of state using the thermodynamic library CoolProp and and the model was written in MatLab language.

Table 3.1.1 lists the equations for the computation of the thermodynamic cycle for the two-stages heat pump studied in this work. The cycle was modeled assuming isobaric condensation and

evaporation, while real expansion and compression with a constant isentropic efficiency.

State Point	Fluid Property	Comments
Evaporator	$p_{evap} = p(T_{evap}, x = 1)$	
Condenser	$p_{cond} = p(T_{cond}, x = 0)$	
State Point 1	$p_1 = p_{cond}$; $T_{1'} = T(p_1, x = 1)$; $T_1 = T_{1'} + \Delta T_{SH}$ $h_1 = h(p_1, T_1)$; $s_1 = h(p_1, h_1)$	
State Point 2	$p_2 = p_1 \cdot \Pi_{stage1}$; $s_{2s} = s_1$; $h_{2s} = h(p_2, s_{2s})$ $h_2 = h_1 + (h_{2s} - h_1)/\eta^{is}_{stage1}$; $s_{2s} = s_1$; $T_2 = T(p_2, h_2)$	
State Point 3	$p_3 = p_2$; $T_{3'} = T(p_3, x = 0)$; $T_3 = (T_{3'} + T2)/2$ $h_3 = h(p_3, T_3)$; $s_3 = h(p_3, T_3)$	First guess of T_3, start of iterations to find real T_3
State Point 4	$s_{4s} = s_3$; $p_4 = p_{cond}$; $\Pi_{stage2} = p_4/p_3$; $h_{4s} = h(p_4, s_{4s})$ $h_4 = h_3 + (h_{4s} - h_3)/\eta^{is}_{stage2}$; $T_4 = T(p_4, h_4)$	
State Point 5	$p_5 = p_4$; $T_5 = T(p_5, x = 0)$; $h_5 = h(p_5, x = 0)$	
State Point 6	$p_6 = p_5$; $T_6 = T_5 - \Delta T_{SC}$; $h_6 = h(p_6, T_6)$	
State Point 7	$h_7 = h_6$; $p_7 = p_3$; $x_7 = Q(h_7, p_7)$; $T_7 = T(p_7, x_7)$	
	$\dot{m}_{stage1} = \dot{m}_{tot}(1 - x_7)$; $\dot{m}_{flash} = \dot{m}_{tot} - \dot{m}_{stage1}$ $T_3 = (\dot{m}_{stage1} T_2 + \dot{m}_{flash} T_{3'})/\dot{m}_{tot}$	Recalculation of T_3, if equal to previous one stops, else continues loop
State Point 8	$p_8 = p_7$; $T_8 = T(p_8, x = 1)$; $h_8 = h(p_8, x = 1)$	
State Point 9	$p_9 = p_8$; $T_9 = T(p_9, x = 0)$; $h_9 = h(p_9, x = 0)$	
State Point 10	$h_{10} = h_9$; $p_{10} = p_1$; $T_{10} = T(p_{10}, h_{10})$ $COP = \frac{\dot{m}_{tot}(h_4 - h_6)}{\dot{m}_{stage1}(h_1 - h_1) + \dot{m}_{tot}(h_4 - h_3)}$	

Table 3.1.1: Equations used to model the heat pump cycle in Matlab using CoolProp library

The calculation passages showed above where then inserted inside a additional series of iterative loops which main function was: (a) stop the iteration when dry compression is not provided anymore, i.e. when the compression transformation line enters the refrigerant bi-phase dome; (b) find the pressure ratio of the first stage delivering the highest COP of the overall cycle. The choice to use a constant isentropic efficiency was done following previous approaches, such as [12] which additionally reported it to be common for theoretical calculations . However, for the present application were different pressure ratio are studies, the use of polytripic efficiency might have been more appropriate since it is independent of the specific pressure ratio. The value of the super-heating of the first stage was set to $\Delta T_{SH} = 5K$, this value was found through an additional iteration process and corresponds to the minimum super-heating required in order to assure a dry compression, i.e. with the refrigerant thermodynamic state never entering inside the bi-phase dome during the compression transformation, consequently guaranteeing the compressor integrity during operation. The value of the sub-cooling used was $\Delta T_{SC} = 20K$ and it is mainly set by the water return temperature of the whole district heating system, hence selected based on the common returning water temperature value in Sweden. The initial value of the isentropic efficiency of the compression was assumed to be 90%, quite higher than the efficiency best performing centrifugal compressors in the market, this efficiency was then re-adapted after the meanline design of the compressors using the efficiency obtained from VISTA CCD results and continuing the iteration until the two efficiencies were found in agreement.

Therefore, a number of iteration between the thermodynamic cycle and the 1D compressor design was required before obtaining the final value for the pressure ratio delivering the highest COP. After this iteration loop was concluded, the final efficiency value settled around 83.5%. The full MatLab code developed can be found in Appendix A. The validation of the model was accomplished comparing with the data resulting from a Siemens in-house generated model of a thermodynamic cycle of a two-stage heat pump. The comparison between the two cycles is shown in Figure 3.1.1, the cycle specifics as well as the values of the cycle points cannot be distributed due to confidential information, hence the axis values were occulted.

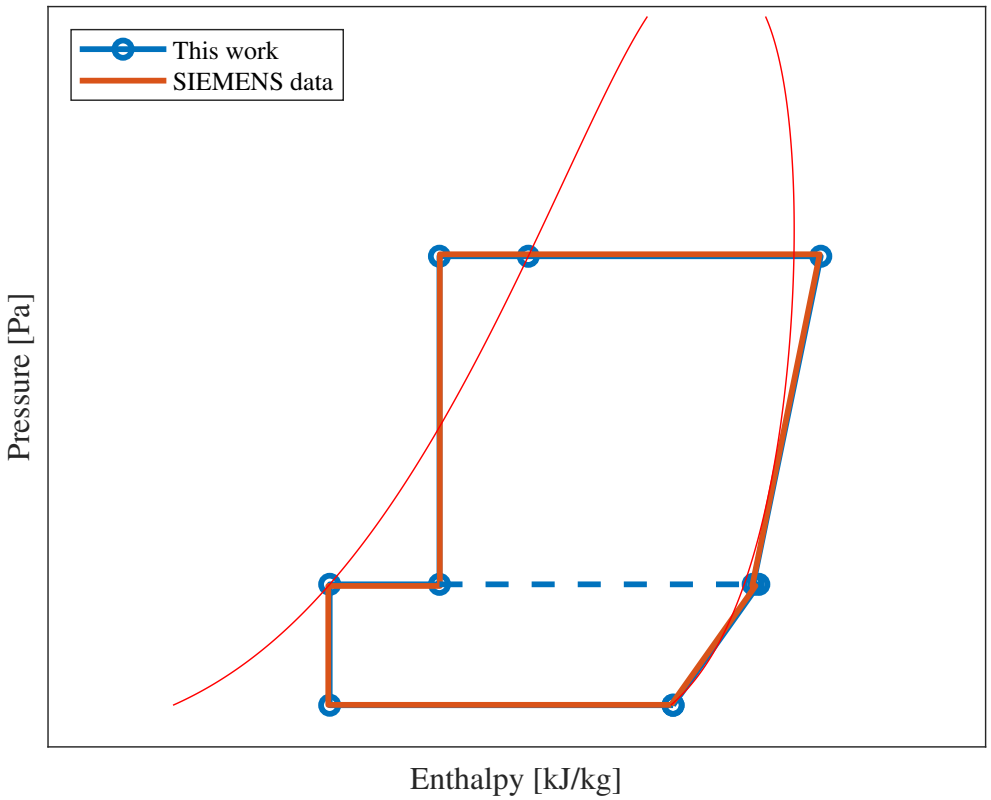

Figure 3.1.1: Comparison between P-h diagrams of a heat pump using R1234ze(E). Data generated with the MatLab code created inside this work are shown in blu, while data coming from Siemens in-house generated model are in red. The values of the cycle are confidential information and were hence occulted.

3.2 Mean-line design of the compressor

In Chapter 2, the most important design parameters, their significance and effects on the final design together with the typical design practices were presented. Table 3.2.1 summarizes these parameters and their values range. The values of the different design parameters were selected starting from the values shown in the above table, then refined with trial and errors methodology, the Direct Optimization tool or simple design choices.

Design variable	Description	Units	Opt. Constraints	Reference
N	Rotational Speed	[rpm]	1500 – 40.000	
$\dot{m}$	Mass flow	[kg/s]	50 – 70	Design specifics
χ_2	Rake angle at trailing edge	[°]	-30 – +30	Drozdov [41]
β_2	Impeller exit blade angle (Backsweep)	[°]	0 – 90	General literature
W_2/W_{1s}	Relative velocity ratio	[-]	0.4 – 0.8	General literature
dc_m/dq	Meridional velocity gradient over the span	[-]	> 1	General literature
m/m_{ch}	Choke margin	[-]	0.8–0.9	Wang et al. [36]
ϕ	Flow coefficient	[-]	0.06 – 0.09	Robinson et al. [32]
ψ	Work coefficient	[-]	0.3 – 1.1	Meroni et al. [2]
M_u	Peripheral mach number	[-]	< 1.6	Sarevski [38]
u_2	Impeller tip speed	[m/s]	< 250	Structural req.
$M_{w1,shroud}$	Relative Mach number at impeller inlet shroud	[-]	0 – 1.4	Meroni et al. [2]
M_{w1}	Relative Mach number at impeller inlet	[-]	0.8 – 0.95	Sarevski - Cumpsty
β_{1s}	Relative flow angle at inlet shroud	[°]	56 – 60	Dixon, Hall [27]

Table 3.2.1: Design variables and typical values used in common practice and state-of-the-art applications

In VISTA CCD, the inputs are divided into three main categories, namely ”Duty and Aerodynamic Data”, ”Gas properties” and ”Geometry”, the setup choices inside these categories will be hence presented in the following three sub-sections:

3.2.1 Duty and Aerodynamic Data

Inside the first tab, the designer can set-up some of the most important parameters for the compressor design. In the present case, some of these parameters were already defined by the thermodynamic cycle, such as the total-to-total pressure ratio of the stage Π_{stage} and the inlet stagnition pressure and temperature $\mathrm{T_{0in}}$ and $\mathrm{p_{0in}}$. Other parameters were selected based on an initial guessed range and then manually optimized with a trial and errors method, for example the rotational speed was selected based on the desired impeller outlet diameter and tip speed, then rounded-off to the closest integer value. Some other parameters where optimized using the Direct Optimization module of VISTA CCD. Finally, some parameters were simply left to their default values. The final setup for the duty and aerodynamics properties tab is presented in Table 3.2.2:

Design variable	Value/Setting	Decision Source
Overall Pressure Ratio [-]	4.4	Thermodynamic cycle
Mass Flow [kg/s]	58.5	Trial and error optimization
Rotational speed [rpm]	9000	Size and structural considerations
Inlet Total Temperature [K]	273	Thermodynamic cycle
Inlet Total Pressure [Pa]	178361.16	Thermodynamic cycle
RMS Inlet Gas angle [°]	0	Default value
Radial distribution method	Free Vortex	Design choice/ General design approach
Choke margin [-]	0.9	Literature
Stage efficiency correlation	Casey-Robinson	Design choice
Reynolds number correction	yes	Default value
Tip clearance and shroud correlation	yes	Default value
Impeller Isentropic efficiency	Link to stage	Default value
Power input factor	Correlation	Default value
Merid. velocity gradient [-]	1.04	Japikse [42]
Relative velocity ratio [-]	0.676	Optimized through Direct Optmization module

Table 3.2.2: Final Setup for the Duty and Aerodynamics Data section in VISTA CCD

3.2.2 Gas properties

Regarding the gas properties, VISTA CCD provides both ideal and real gas models. Inside both of this models a short library of refrigerants is accessible, however R1234ze(E) is not present in this list and the user has to specify the properties manually. In a first instance, it was explored the possibility to use the ideal gas model option, here the user has to insert only the gas constant R, the specific heats ratio γ and the viscosity, dynamic μ or kinematic ν, this model would have allowed to reduce the degree of complexity of the setup, saving computational effort and time. However, comparing the ideal model results with the ones obtained using the real model it was observed that the two designs were significantly different. In particular, the main difference was lying in the outlet section of the impeller. Indeed, in the ideal gas model the gas properties are assumed constant throughout the whole stage, hence the average properties should be used. However, due to the big difference of pressure and temperature between inlet and outlet the gas properties are changing drastically along the stage and using average properties ends up negatively affecting the design, especially in the outlet section were the gas density plays an important role in the definition of the section width, that if not properly designed could ultimately lead to unexpected premature choking. Moreover, even though for the first stage design the ideal gas model could provide admissible results, the second stage was operating at outlet conditions very close to the critical point, where the specific heats of the refrigerant have particular behaviours, such as sudden and very significant increase. Considering average values in such case would have meant to design the inlet and outlet of the impeller with conditions that are actually very far from the true local values.

Therefore, it was decided to use the real gas model, this requires the user to insert additional gas properties such as critical pressure, temperature and specific volume together with the acentric factor, these parameters were again obtained from the CoolProp library. Additionally, it is

required to define the correlation between the specific heat at constant pressure c_p and the temperature, this is done inserting the polynomial coefficients of polynomial approximation of the function $c_p = f(T)$. The final setup of the Gas properties tab is presented in Table 3.2.3:

Design variable	**Value**
Gas constant R_g [J/(kg K)]	72.907
Dynamic viscosity μ [Pa s]	$1.231 \cdot 10^{-5}$
Critical pressure [Pa]	3634900
Critical temperature [K]	382.5
Critical specific volume [m^3/kg]	0.002
Acentric factor [-]	0.313
c_p polynomial correlation	$c_p = 3.12 \cdot 10^2 + 2.16\ \mathrm{T} - 9.15 \cdot 10^{-4}\ \mathrm{T}^2$

Table 3.2.3: Final Setup for the Gas properties section in VISTA CCD

3.2.3 Geometry

The geometric properties section is responsible for the setup of the most important geometric parameters, from impeller size to the number of blades, to the backsweep angle etc. The common range of values of most of these properties in state-of-the-art designs was already shown in Table 3.2.1. Starting from these ranges a great trial and error procedure was applied in order to find a suitable value for some of these parameters, while the inducer hub diameter and backsweep angle final values were selected applying a parametric optimization using the Direct Optimization module. For the reasoning explained in Chapter 2, a vaneless diffuser was selected. The number of blades was selected using the correlation presented by Xu and Amano [35] that correlates the total number of blades (main blades plus splitters) with the total-to-total pressure ratio, for the present application the number of blades calculated is 25.3, since the total number should be even, i.e. same number of full blades and splitters, these was rounded up to 26, also in order to assure a lower blade-loading. Other parameters were left to their default values. The final setup used for the geometric properties tab is shown in Table 3.2.4. As anticipated above, the Direct Optimization module was ultimately used on three parameters, namely the inducer hub diameter, the backsweep angle and the relative velocity ratio. The optimization method was set to Manual and the Screening method was utilized, this is a multi-objective method and it is typically used to find a first set of candidate points for a preliminary design. A number of 100 design points was considered a good trade-off between accuracy and computational time, among these points only three were selected as candidate points, these are the three points that maximize the efficiency still remaining inside the constraints imposed or meeting the desired objectives. In a first instance, a high number of objectives and constraints was used, but experience have shown that minimizing this number have several benefits on the optimization procedure, such as a reduction in the computational effort together with a more accurate search. The setup of the Direct Optimization tool is shown in Table 3.2.5.

Design variable	Value/Setting	Decision Source
Inducer Hub		
Diameter [mm]	152.4	Optimized through Direct Optimization
Vane inlet angle	Unchecked	Default value
Vane normal thickness [mm]	3	Xu & Amano [35]
Inducer Shroud		
Diameter (specified) [mm]	378	Design choice
Vane inlet angle	Unspecified	Default value
Vane normal thickness [mm]	2	Xu & Amano [35]
Leading edge		
Location on shroud [%]	0	Default value
Normal to hub option	Unchecked	Default value
Angle of Inclination [°]	0	Default value
Diffuser		
Tipe of vane	Vaneless	Design choice
Impeller shroud and clearance		
Tipe of shroud	Unshrouded	Default value
Tip clearance/vane height	0.03	Default value
Axial lenght ratio		
Tipe of calculation	Automatic	Default value
Other impeller geometry		
Number of blades - Main	13	Xu & Amano [35]
Number of blades - Intervanes	13	Xu & Amano [35]
Rake angle [°]	30	Drozdov et al. [41]
Vane roughness	Machined finish	Default value

Table 3.2.4: Final Setup for the Geometry section in VISTA CCD

Objective/Constraints Parameters	Target	Lower boundary	Upper boundary
Isentropic efficiency	>85%	83%	Not defined
Impeller outlet diameter [mm]	492	Not defined	Not defined
Optimization Parameters	**Target**	**Lower boundary**	**Upper boundary**
Backsweep angle [°]	Not defined	40	70
Relative velocity ratio [-]	Not defined	0.5	0.7
Inducer hub diameter [mm]	Not defined	130	170

Table 3.2.5: Final Setup for the Geometry section in VISTA CCD

The project schematic in Ansys WorkBench of the mean-line design of the first stage is showed in Figure 3.2.1.

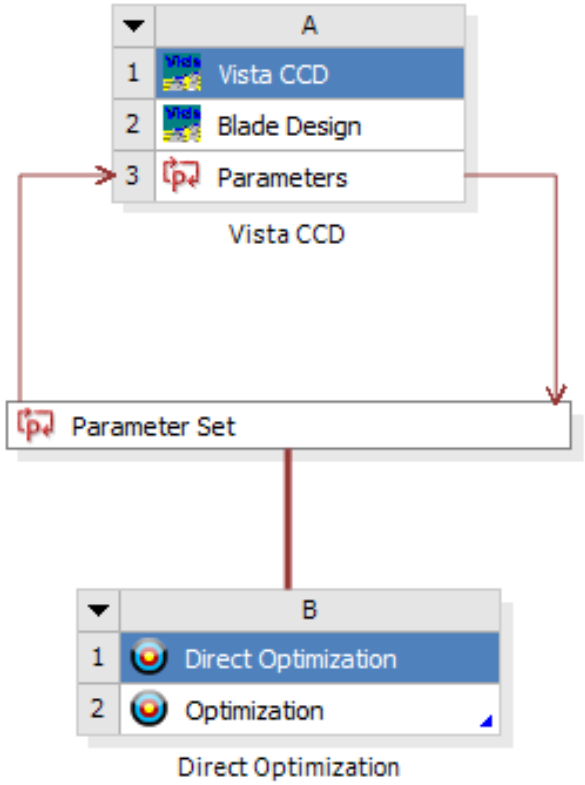

Figure 3.2.1: Project schematic of the mean-line design in Ansys WorkBench using VISTA CCD coupled with the Direct Optimization module

3.3 3D design and CFD

After the mean-line design of the impeller was completed it could be imported into the BladeGen module in order to start the 3D design and following CFD simulations. The first step was hence to modify the diffuser shape so that it could provide the performances required. The diffuser outlet radius was first calculated using the correlation from [56], which correlates the diffuser outlet radius with the with the impeller outlet ratio and flow coefficient. Additionally, the inlet of the fluid domain was extended of one axial length in order to have an already developed steady flow at the inlet of the impeller. Once this step is completed, the final 1D design was transformed into a 3D design linking the BladeGen module with a TurboGrid module. In order to reduce the computational effort, the machine was divided in 13 sectors, each composed by a full blade and a splitter blade, and the simulation domain was defined by one single sector. The computational grid (or mesh) was generated in ANSYS Turbogrid and a convergence study was assessed, four meshes were generated and it was monitored the convergence of both the mass flow ratio and the isentropic efficiency, Figure 3.3.1 shows the variance between the results obtained with different mesh densities for mass flow and isentropic efficiency, where the benchmark mesh is the one with the highest number of nodes. Since the difference between the finest and second finest mesh is almost negligible, about 0.5% for the mass flow and 0.09 % for the isentropic efficiency, the simulations could be considered grid independent and the mesh with $1.36 \cdot 10^6$ elements was

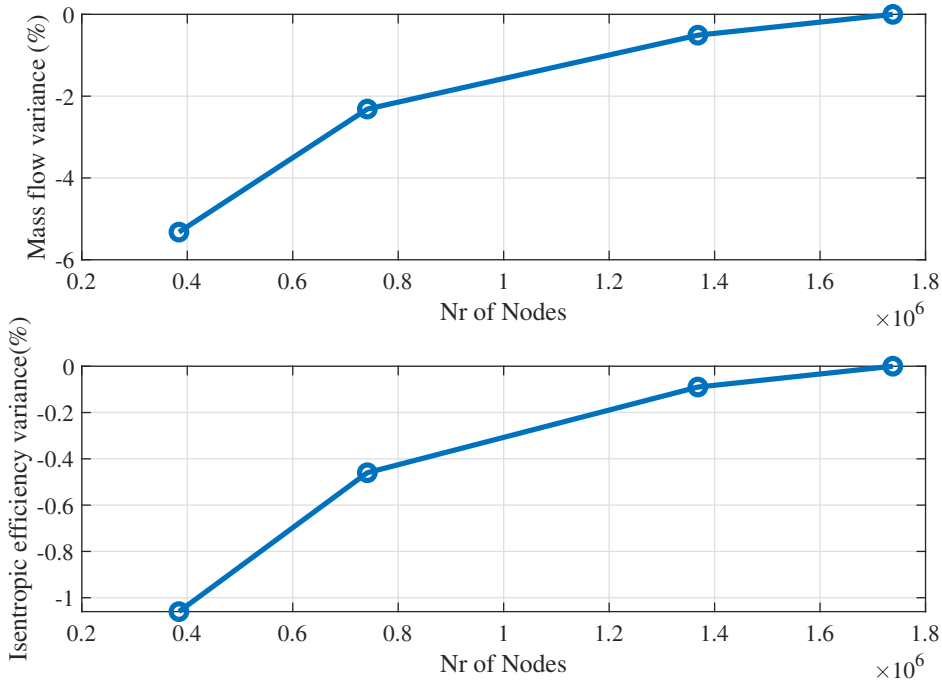

Figure 3.3.1: Variance between different mesh densities for mass flow (Top) and isentropic efficiency (Bottom), the benchmark mesh is the one with the higher number of nodes.

considered the best trade-off between computaional time and accuracy, hence selected as new benchmark mesh for the continuation of the study. The Mesh Data main parameters settings used to generate the benchmark grid are shown in Table 3.3.1, the parameters not specified should be considered as their default or automatically generated values.

Mesh Size	
Method	Global size factor
Size Factor	1.4
Boundary Layer Refinement Control Method	Proportional to Mesh size
Near Wall Element Size Specification Method	Absolute
Passage	
Method	Element Count and Size
Nr. of Elements	30
Const Elements	15
Size of Elements Next to Wall	0.005 mm

Table 3.3.1: Final Setup for the Geometry section in VISTA CCD

The benchmark mesh ultimately used after the mesh independence study is shown in Figure 3.3.2:

Once a suitable mesh was generated, the TurboGrid module was finally linked to a CFX module and the Turbo Mode tool inside CFX-Pre was used to setup of the CFD simulations of the centrifugal compressor. The final project schematic for the 3D CFD part of the work is shown

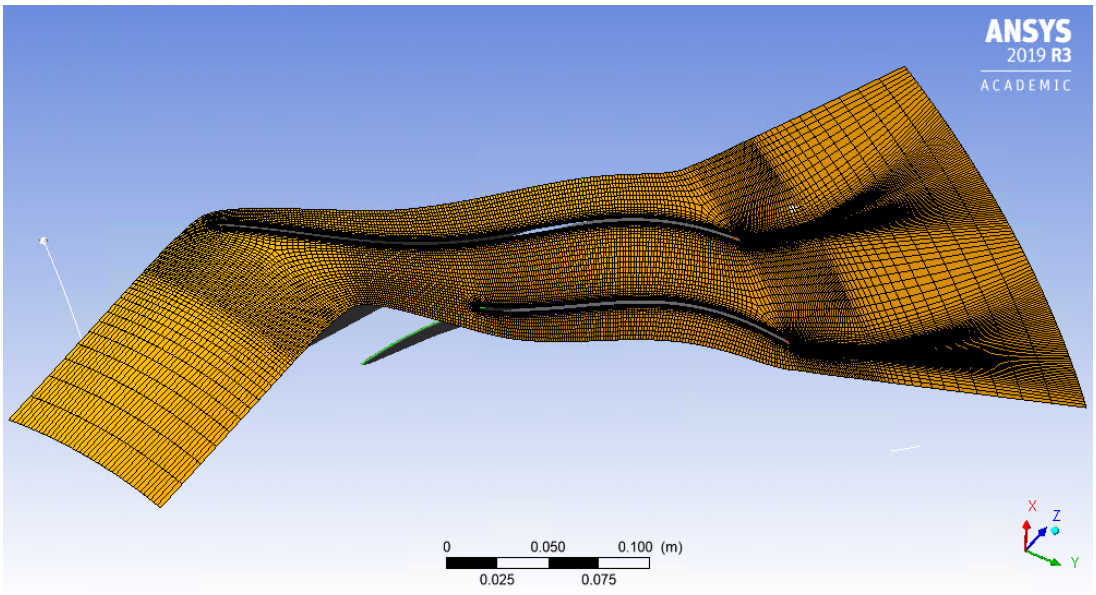

Figure 3.3.2: Benchmark mesh used for the CFD simulations, obtained with the setup of Table 3.3.1

in Figure 3.3.3. Inside the Turbo Mode, a steady state analysis type was selected, with a

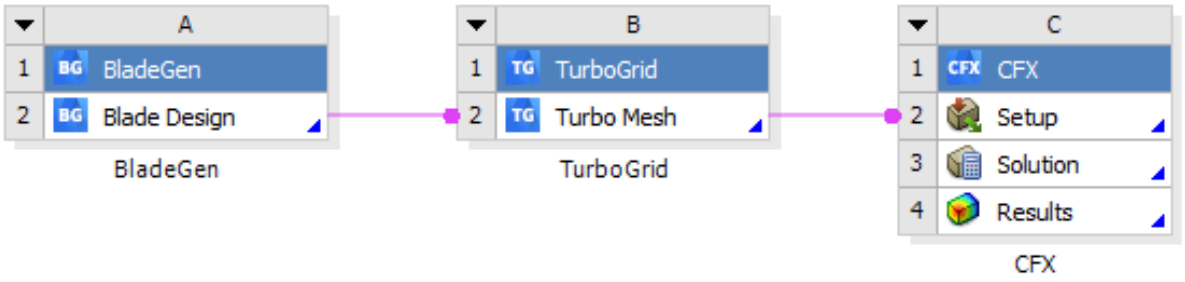

Figure 3.3.3: Project Schematic for the 3D CFD part of the work

Total Energy heat transfer method and a $k-\omega$ SST turbulence model, that as anticipated in 2 is considered the most appropriate choice for turbomachinery applications, deliverying the most realistic results, as identified by [43] and [49]. Following Rinaldi [49] and Li [57], the computational domain was partitioned into the stationary inlet, rotating impeller, and stationary diffuser, with Stage (or Mixing-Plane) interfaces between adjacent domains, while the interfaces between adjacent axisymmetric sectors were set as periodic. The rotational speed of -9000 rpm with respect to the Z-axis was imposed only to the rotating domain representing the impeller. The Normal to Boundary option was selected as flow direction. The boundary conditions used were P-total inlet and P-static at outlet, as specfied in the Ansys CFX-Pre User's Guide [58] this is a very robust method to impose boundary conditions in turbomachinery design. The boundaries different from inlet or outlet were all imposed with a No Slip Wall condition, except for the wall corresponding to the rotating subdomain shroud, which in fact was set as Counter Rotating. Regarding the refrigerant, R1234ze(E) was not present in the CFX library and its properties had to be imported manually, at first it was explored the possibility of directly importing an RGP file

generated through the REFPROP library and a python interface, however this method brought to immediate divergence of the simulations, but the source of the issue could not be identified. Therefore, the refrigerant was imported using the material creation option in Ansys CFX-Pre, and the material setup used is shown in Table 3.3.2, all the parameters not specified should be considered with their default values.

Basic Settings	
Option	Pure Substance
Material Group	Redlich Kwong Dry Refrigerants
Thermodynamic State	Gas
Material Properties	
Option	General Material
Equation of State	
Option	Real Gas
Model	Aungier Redlich Kwong
Molar Mass	0.114 [kg/mol]
Critical Temperature	382.52 K
Critical Pressure	3634936.85 [Pa]
Critical Volume	0.0002331 [m^3/mol]
Acentric Factor	0.313
Boiling Temperature	247.08 K
Specific Heat Capacity	
Zero Pressure Coeff. option	Fourth Order Polynomial
a1	1.98149
a2	0.0555617 [K^{-1}]
a3	-0.000118091 [K^{-2}]
a4	$1.82803 \cdot 10^{-7}$ [K^{-3}]
a4	$-1.14464 \cdot 10^{-10}$ [K^{-3}]
Lower $C_{p0(T)}$ Temperature Limit	200 K
Upper $C_{p0(T)}$ Temperature Limit	600 K
Table Generation	
Minimum Temperature	200 K
Maximum Temperature	600 K
Minimum Absolute Pressure	50000 [Pa]
Maximum Absolute Pressure	$2 \cdot 10^6$ [Pa]
Temperature Extrapolation	Active
Pressure Extrapolation	Active
Transport Properties	
Dynamic Viscosity	Checked
Option	Kinetic Theory Model
Dynamic Viscosity Model Option	Rigid Non Interacting Sphere
Thermal Conductivity	
Option	Kinetic Theory Model
Thermal Conductivity Model Option	Modified Eucken

Table 3.3.2: Material Setup in Ansys CFX-Pre for R1234ze(E)

The Turbo Mode final setup used is presented in Table 3.3.3, while the simulation domain is shown in Figure 3.3.4.

Basic Settings	
Machine Type	Centrifugal compressor
Coordinate Frame	Coord 0
Rotation Axis	Z
Analysis type	Steady State
Components Definition	
Inlet	Stationary
Impeller	Rotating (-9000 rpm)
Outlet	Stationary
Physics Definition	
Fluid	R1234ze(E)
Reference Pressure	0 Pa
Heat Transfer	Total Energy
Turbulence	Shear Stress Transport
Boundary Conditions option	P-Total Inlet ; P-Static Outlet
Flow direction	Normal to Boundary
Default Interface Type	Stage (Mixing-Plane)

Table 3.3.3: Turbo Mode setup in Ansys CFX-Pre

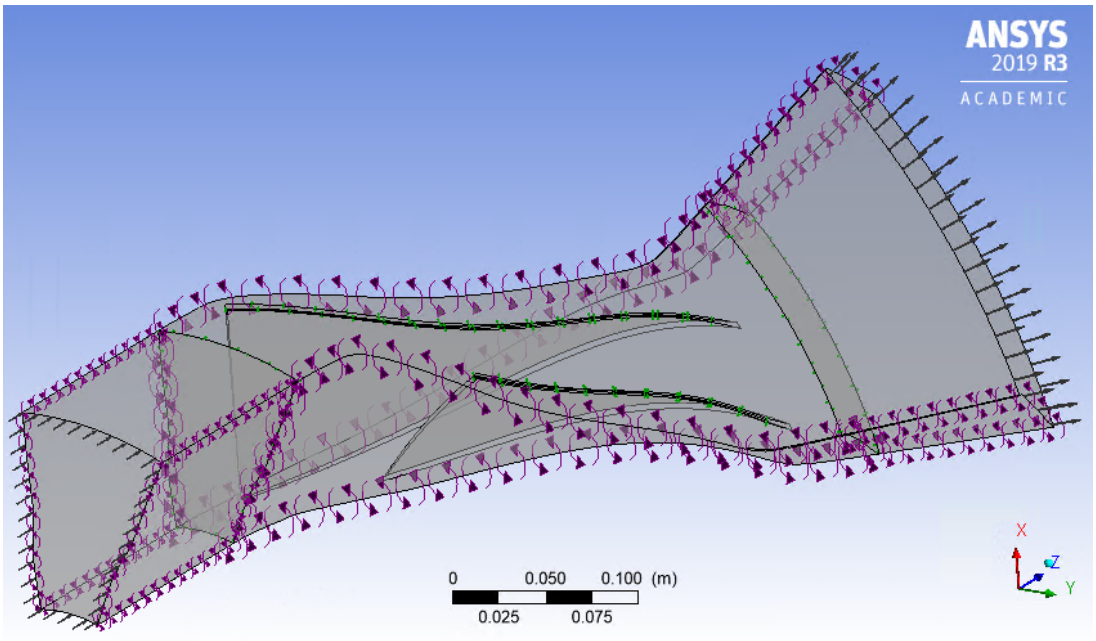

Figure 3.3.4: CFD simulation domain partitioned into the stationary inlet, rotating impeller, and stationary diffuser

Chapter 4

Results & Discussion

Chapter 3 explained the methodology followed in the design process of the heat pump model and the first stage of the centrifugal compressor. In this chapter, the results obtained will be presented and discussed.

4.1 Heat Pump Thermodynamic cycle

First of all, one should observe the correlation between the COP and the pressure ratio of the first stage, remembering that the selection of the latter automatically fixes the pressure ratio of the second stage. The relation between COP and Π_{stage1} is shown in Figure 4.1.1 below:

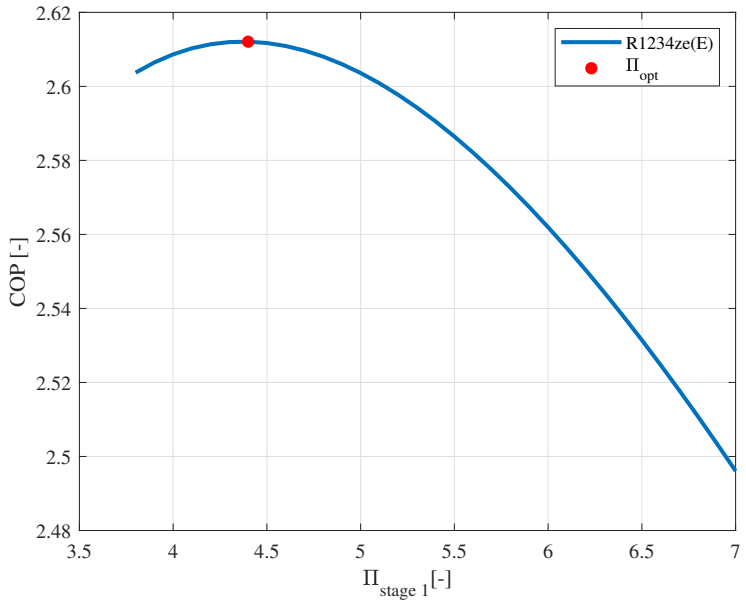

Figure 4.1.1: Coefficient of Performance (COP) as function of the pressure ratio of the first stage for a heat pump with R134ze(E), $T_{evap} = -5°C$, $T_{cond} = 100°C$, $\Delta T_{SH} = 5°C$, $\Delta T_{SC} = 20°C$, $\eta^{is}_{stage1} = \eta^{is}_{stage2} = 83.5\%$

It was already explained in the previous chapters that the final isentropic efficiency η^{is}_{stage1} of 83.5% used in the thermodynamic cycle is the result of an iteration between the cycle and the 1D meanline design, the efficiency of the second stage was temporarily assumed to be equal to the one of the first stage, although a correct design should favor higher efficiency in the second stage as it has a higher mass flow.

From Figure 4.1.1, it can be observed that the final optimum pressure ratio of the first stage was found to be $\Pi^{\text{opt}}_{\text{stage1}} = 4.4$, consequently fixing the second stage pressure ratio at a lower pressure ratio of $\Pi^{\text{opt}}_{\text{stage2}} = 3.84$. This result could have been predicted a priori since the corrected speed of the second stage, for same size and rotational speed, must be lower compared to the first stage due to the higher total temperature at the inlet. However, it also finds practical benefits as explained by [42], since the second stage has a higher mass flow it will experience higher structural and aerodynamic loads and more power required compared to the first stage, it is therefore desirable to have a lower pressure ratio on this stage in order to reduce such loads and to increase efficiency. As can be observed, for such pressure ratios the COP obtained is equal to 2.61 and here it comes one of the main outcomes of this work; in most of the works present in literature the variation of COP is generally studied for fixed pressure ratio and varying temperature lifts, and it was showed ([17], [59]) that for increasing temperature lifts the COP of the cycle tends to decrease. In the present work, a different approach was used and variation of the COP for a fixed temperature lift was studied the for a varying pressure ratio, showing that for a given refrigerant it exist a very specific intermediate pressure level of the heat pump, corresponding to the pressure ratio of the first stage, that delivers the highest performances of the cycle. Arpagaus et al. [17] showed the correlation between the COP and the temperature lift for 20 heat pumps present in industry, comparing these heat pumps with the one designed in the present work two main considerations can be be drawn. First of all very few applications present temperature lifts of 100 K or more, the heat pump with 105 K temperature lift explored in this work has therefore to be considered as a cutting edge technology. Secondly, the optimization of the pressure ratio clearly adds significant benefit to the overall performances of the heat pump since the COP of 2.61 obtained in the present work is significantly higher compared to heat pumps with similar temperature lifts. The comparison between the present work results and the other heat pumps present in industry as shown by [17] is shown in Figure 4.1.2, while Figure 4.1.3 presents the final thermodynamic cycle obtained for pressure ratios specified above.

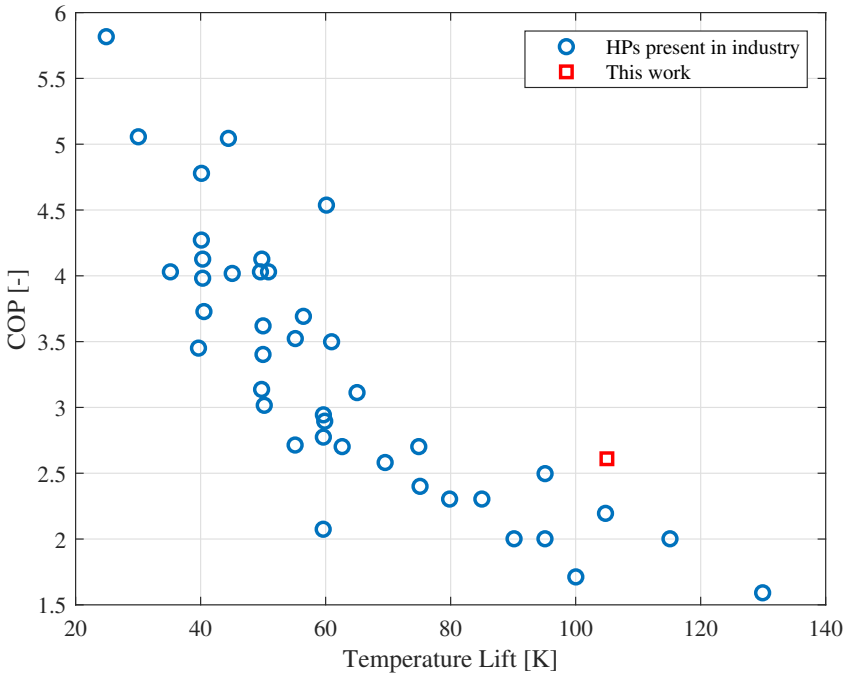

Figure 4.1.2: COP of various industrial HPs as a function of the temperature lift (blu circles as presented by [17]), compared with the theoretical results of the HTHP designed in the present work (red square).

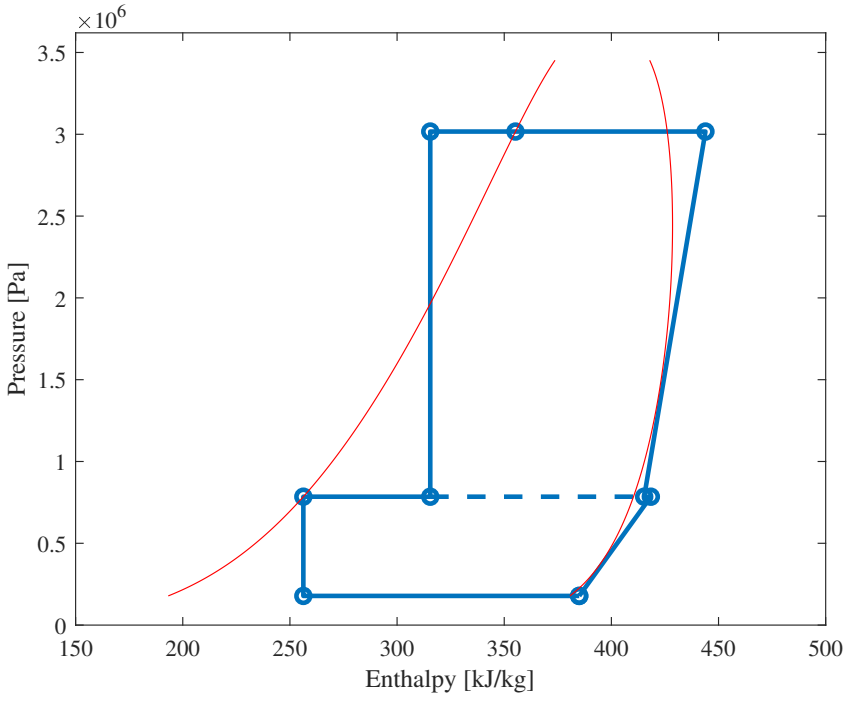

Figure 4.1.3: Final thermodynamic cycle for a heat pump with R134ze(E), $T_{evap} = -5°C$, $T_{cond} = 100°C$, $\Delta T_{SH} = 2°C$, $\Delta T_{SC} = 20°C$, $\eta^{is}_{stage1} = \eta^{is}_{stage1} = 83.5\%$ and pressure ratios $\Pi^{opt}_{stage1} = 4.4$, $\Pi^{opt}_{stage2} = 3.84$.

4.2 Mean-line design of the compressor

The resulting mean-line design for the first stage of the compressor obtained in VISTA CCD with the setup presented in Chapter 3 is shown in Figure 4.2.1 in its impeller sketch and efficiency plot. The black square in the efficiency plot represents the design point, the compressor was

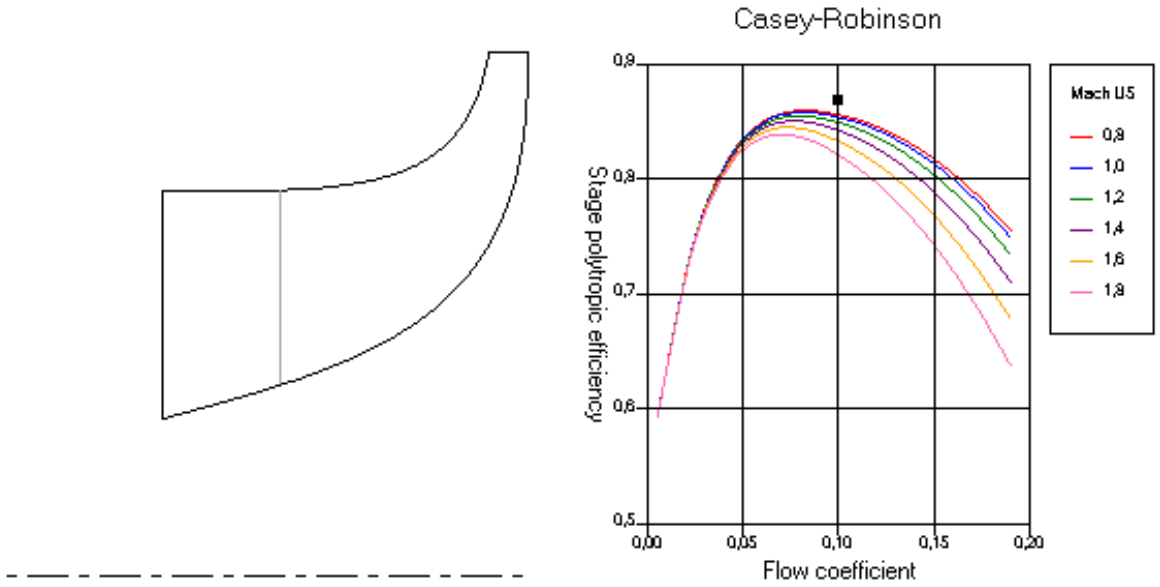

Figure 4.2.1: Impeller sketch (left) and efficiency plot (right) of the first stage of the compressor as shown in VISTA CCD output

intentionally designed at a design point that falls on the right hand side of the peak of maximum efficiency, this is done to assure more stable performances and to avoid to obtain too low flow coefficients on the second stage, again remembering that this will have the same size and rotational speed but a higher mass flow. The main output parameters obtained in VISTA CCD are shown in Table 4.2.1.

Impeller leading edge	
Meridional velocity ratio [-]	1.04
Relative velocity ratio [-]	0
RMS Mach Nr.	0.587
RMS Absolute Velocity [m/s]	82.65
Throat Area [mm^2]	50981.7
Total Enthalpy [kJ/kg]	194.23
Inclination [°]	0
Relative Mach number at Hub [-]	0.746
Relative Mach number at RMS [-]	1.12
Relative Mach number at Shroud [-]	1.39
Impeller exit	
Diameter [mm]	509.23
Tip width [mm]	18.67
Total Temperature [K]	323.67
Total Pressure [Pa]	888.81
Total Enthalpy [kJ/kg]	228.69
Impeller speed [m/s]	239.97
RMS Mach Nr. [-]	1.109
RMS Relative velocity [m/s]	132.2
RMS Absolute velocity [m/s]	164.32
RMS Absolute flow angle α [°]	58.3
RMS Relative Flow angle β [°]	49.2
Relative velocity ratio [-]	0.68
Overall Performance	
Specific speed	1.057
Flow coefficient ϕ	0.099
Work coefficient ψ	0.599
Power required [kW]	2016.23

Table 4.2.1: Main output values of the meanline stage design obtained in VISTA CCD.

As explained in Chapter 3, the mean-line design had to be adjusted modifying the diffuser outlet radius and extending the inlet channel. The the final mealine design obtained in BladeGen, comprehensive of inlet flow channel, impeller and diffuser has an axial length of 357 mm and an outlet diameter of 869 mm and is shown in Figure 4.2.2:

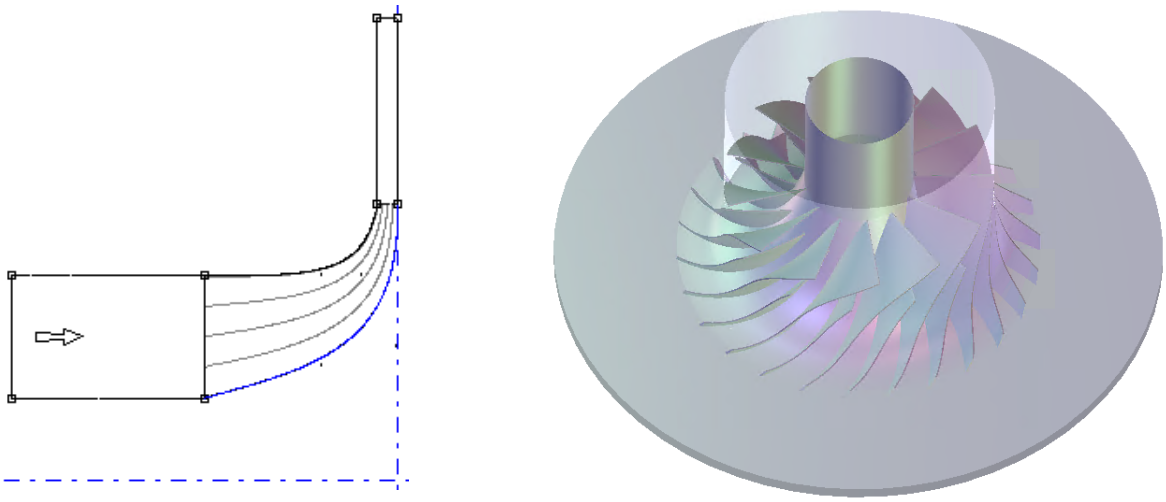

Figure 4.2.2: Full 1D meanline design, comprehensive of inlet flow channel, impeller and diffuser (Left), and full 3D impeller rendering (Right) as obtained in BladeGen.

4.3 3D design and CFD

The CFD results now need to confirm all the predictions made by the thermodynamic cycle and meanline preliminary design, proving that this specific design is feasible and that the performances of the compressor are satisfactory. The parameters of main interest in the CFD results were hence the ones strictly related to the thermodynamic cycle of the heat pump, i.e. total temperature at outlet, pressure ratio across the compressor, mass flow and efficiency, the output values of these parameters obtained through CFD are shown in Table 4.3.1.

3D CFD Results	
Mass flow [kg/s]	55.88
Pressure ratio [-]	4.409
T_0 at Imp. outlet [K]	323.8
Efficiency [%]	80

Table 4.3.1: 3D CFD simulations Main results

The static temperature and pressure variation throughout the simulation domain at midspan are shown in Figure 4.3.1 and 4.3.2 below:

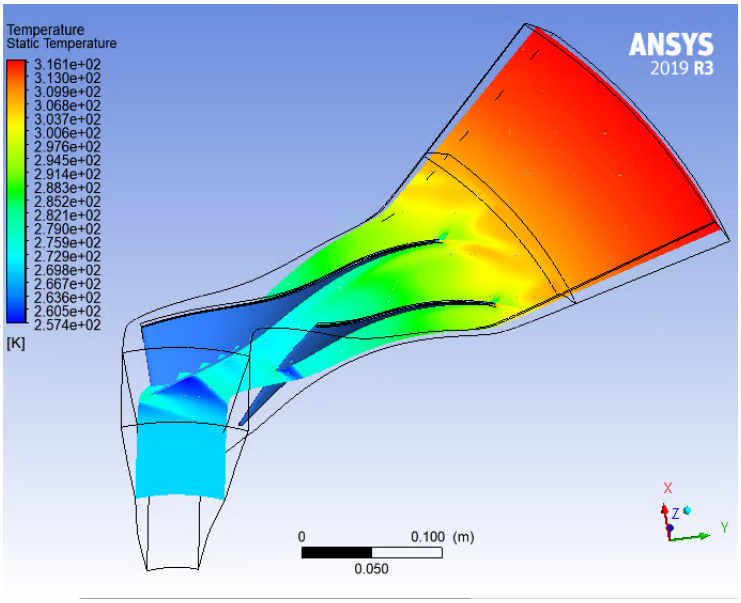

Figure 4.3.1: Static Temperature variation at midspan throughout one sector of the compressor stage.

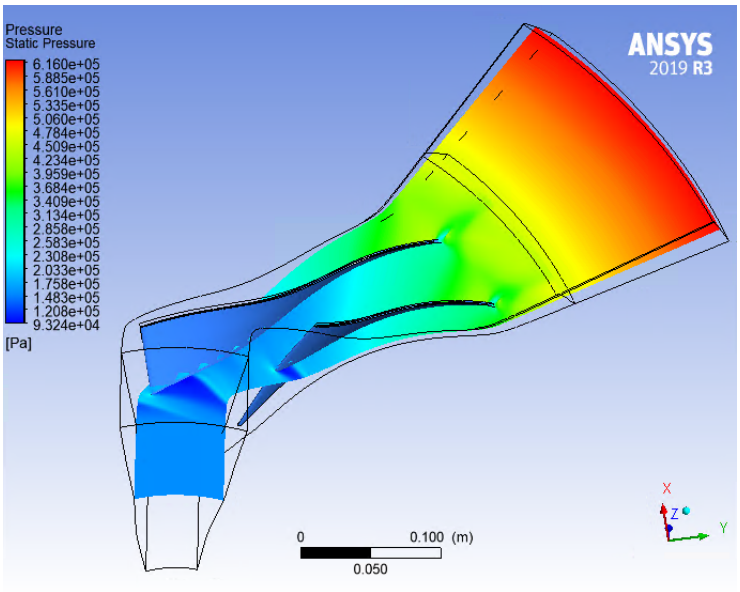

Figure 4.3.2: Static Pressure variation at midspan throughout one sector of the compressor stage.

Finally, the performances of the centrifugal compressor stage were assessed, this is generally done plotting the pressure ratio as function of the normalized mass flow $\dot{m}\sqrt{T_{01}}/p_{01}$. For a given rotational speed, the line representing such relation terminate on the left hand side at the stability line (or surge or stall line) and beyond this point the operation is considered unstable, while on the right hand the curve becomes vertical and no further increase in the normalized mass flow is possible, meaning that the Mach number across a section of the machine reached the unit and the flow is hence choked. The compressor is able to operate anywhere between the surge and choking point, however it is usually constrained to a single design (or operating) point. The performance curve and the operating point of the compressor first stage running

at 9000 rpm is showed in Figure 4.3.3. It should be observed that an increase in compressor

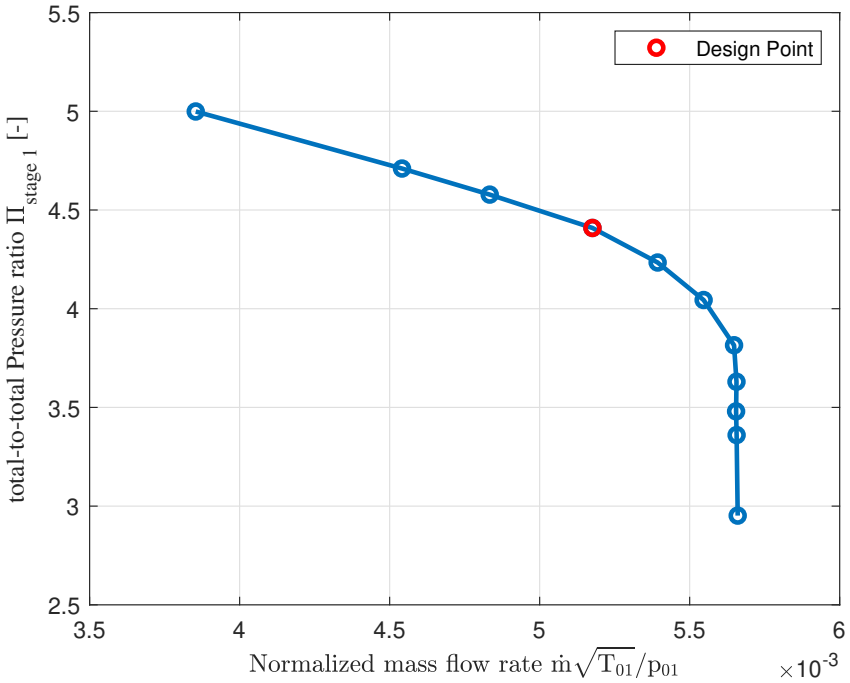

Figure 4.3.3: Performance map for the first stage of the centrifugal compressor operating at a rotational speed of 9000 rpm

pressure ratio can be obtained by reducing the compressor mass flow rate. As reminded by [60], this has to be expected because an increase in pressure at compressor delivery can only be expected if there is a resistance to flow, otherwise, the compressor would behave more like a fan or a blower. Additionally, to avoid surge and rotating stall it is necessary for the stage to have a falling pressure rise characteristic with increasing flow, and this is the main reason why back-sweep is used, to provide an inherently stable form of characteristic with rising pressure as the flow is reduced. In CFD, the stall line is generally found when the numerical simulations start diverging or the main output parameters present significant fluctuations, while choking is identified by the mass flow rate vertical asymptote. The choking was identified to happen at a mass flow around 115% of the nominal mass flow, corresponding to 65 kg/s, while the surge seem to happen around 49.5 kg/s, at a mass flow 85% of the nominal one. This result addresses another of the main challenges present in the field of heat pumps after the improvement of the COP. Indeed, an appropriate turbocompressor for driving heat pumps with a high temperature lift requires the ability to operate on a wide range of pressure ratios and mass flows, generally requiring the designer to make a compromise between range and efficiency. Previous results, such as the ones from Mehra et al. [61], also presented pressure ratios of 4.4 and wide operating range but delivered an efficiency around 63%. The present work can deliver pressure ratios and mass flows up to 115 % and low to 85% of the nominal value before choking, still presenting very satisfying efficiencies about 80% in the whole range.

Chapter 5

Conclusions

The present work presented a complete procedure for the design of the first stage of a centrifugal compressor for heat pumps, starting from the thermodynamic cycle, then moving to the preliminary 1D meanline design and finally concluding with the 3D design and CFD simulations. The main aim of the work was to address some of the current industry's goals in the field of heat pumps, in particular the one and main achievement of the present work has been to design the first stage of a centrifugal compressor for a heat pump with a temperature lift of $105°C$ and that could outperform current existing heat pumps in terms of COP. To do so, a MatLab code able to find the optimum pressure ratio distribution was built and the compressor stage was designed accordingly. The results have proven that, for a fixed temperature lift, a correct distribution of pressure ratio can significantly improve the heat pump performances, reaching a COP of 2.61. Moreover, the results obtained in all the phases of the project were in agreement between each other as it is shown in Table 5.0.1, meaning that the requirement imposed by the thermodynamic cycle can be met, at least in a numerical simulation environment. It can be observed that

	Thermodynamic Cycle	**Mean-line design**	**3D CFD**
Mass flow [kg/s]	58.5	58.5	55.88
Pressure ratio [-]	4.4	4.4	4.409
T_0 at Imp. outlet [K]	322.3	323.7	323.8
Efficiency [%]	83.5	83.5	80.3

Table 5.0.1: Comparison between the main output control values for the thermodynamic cycle, meanline design and CFD simulations

a very good agreement is found between all the three design phases, while the results of the thermodynamic cycle and meanline are close to complete matching a slight difference between the CFD results was found regarding the mass flow and efficiency, however, the maximum variance is in the order of 4.6 % for the mass flow and 3.6 % for the efficiency, hence the results were considered satisfactory. Additionally, the centrifugal compressor design, not only was able to satisfy the conditions imposed by the thermodynamic cycle, but also addressed another of the

main challenges present in the field. Indeed, an appropriate turbocompressor for driving heat pumps with a high temperature lift requires the ability to operate on a wide range of pressure ratios and mass flows, generally requiring the designer to make a compromise between range and efficiency. The present work, thanks to the coupling between thermodynamic cycle and compressor design and their optimization, has designed a centrifugal compressor able to deliver good performances still providing a quite wide operating range.

Still, many improvements can be made and the scope of the whole study can be greatly extended. First of all, the design of the second stage is required to totally validate the results obtained until now, the feasibility of this stage is a critical aspect for the actual realization of the heat pump. In the thermodynamic cycle, a change in use from isentropic to polytropic efficiency can be done. Additionally, the study can be replicated using other refrigerants, the MatLab code constructed is able to run with several other refrigerants present in the CoolProp library and it was already observed that R123ze(E) actually presents one of the lowest COP compared to other refrigerants with better environmental effects, such as Ammonia, for a heat pump with the same temperature lifts. However, different refrigerants have different pressure ratio optimum distribution, hence different compressor designs. Future research topics might consider to design centrifugal compressors for different refrigerants observing if the performance predictions made by the MatLab code are further validated and if the compressor operating range and efficiency are still satisfying.

Finally, as the climate and environmental issues are becoming a central topic of discussion, the energy saving and optimization is becoming a requirement and heat pumps are regarded are a very attractive and promising solution to solve this issues, event though they offer suitable applications to a vast a variety of other fields. A good amount of research has been devolved to heat pumps in the last decades and this trend seems to be increasing significantly in the last years but there is still a lack of studies regarding high temperature heat pumps with temperature lifts higher than 100 K, and among these studies very few have been coupling the compressor design with thermodynamic cycle, and even when this happens the compressor design is generally reduced to 1D meanline design. This work could serve as a starting point for future students or professionals that would like to further investigate high temperature heat pumps and their performance optimization considering the inter-dependency between thermodynamic cycle and compressor design.

Bibliography

[1] *Iea: Heat pumps in district heating and cooling systems*, https://www.iea.org/articles/heat-pumps-in-district-heating-and-cooling-systems.

[2] Meroni, A., Zühlsdorf, B., Elmegaard, B., and Haglind, F., "Design of centrifugal compressors for heat pump systems," *Applied Energy*, vol. 232, pp. 139–156, 2018, ISSN: 0306-2619. DOI: https://doi.org/10.1016/j.apenergy.2018.09.210. [Online]. Available: https://www.sciencedirect.com/science/article/pii/S0306261918315290.

[3] Domanski, P. A., Steven Brown, J., Heo, J., Wojtusiak, J., and McLinden, M. O., "A thermodynamic analysis of refrigerants: Performance limits of the vapor compression cycle," *International Journal of Refrigeration*, vol. 38, pp. 71–79, 2014, ISSN: 0140-7007. DOI: https://doi.org/10.1016/j.ijrefrig.2013.09.036. [Online]. Available: https://www.sciencedirect.com/science/article/pii/S0140700713002703.

[4] McLinden, M. O., Kazakov, A. F., Steven Brown, J., and Domanski, P. A., "A thermodynamic analysis of refrigerants: Possibilities and tradeoffs for low-gwp refrigerants," *International Journal of Refrigeration*, vol. 38, pp. 80–92, 2014, ISSN: 0140-7007. DOI: https://doi.org/10.1016/j.ijrefrig.2013.09.032. [Online]. Available: https://www.sciencedirect.com/science/article/pii/S0140700713002661.

[5] Kondou, C. and Koyama, S., "Thermodynamic assessment of high-temperature heat pumps using low-gwp hfo refrigerants for heat recovery," *International Journal of Refrigeration*, vol. 53, pp. 126–141, 2015, ISSN: 0140-7007. DOI: https://doi.org/10.1016/j.ijrefrig.2014.09.018. [Online]. Available: https://www.sciencedirect.com/science/article/pii/S0140700714002576.

[6] Schiffmann, J., "Integrated Design and Multi-objective Optimization of a Single Stage Heat-Pump Turbocompressor," *Journal of Turbomachinery*, vol. 137, no. 7, Jul. 2015, 071002, ISSN: 0889-504X. DOI: 10.1115/1.4029123. eprint: https://asmedigitalcollection.asme.org/turbomachinery/article-pdf/137/7/071002/6301835/turbo_137_07_071002.pdf. [Online]. Available: https://doi.org/10.1115/1.4029123.

[7] Schiffmann, J. and Favrat, D., "Design, experimental investigation and multi-objective optimization of a small-scale radial compressor for heat pump applications," *Energy*, vol. 35, no. 1, pp. 436–450, 2010, ISSN: 0360-5442. DOI: https://doi.org/10.1016/j.energy.2009.10.010. [Online]. Available: https://www.sciencedirect.com/science/article/pii/S0360544209004435.

[8] Javed, A., Arpagaus, C., Bertsch, S., and Schiffmann, J., "Small-scale turbocompressors for wide-range operation with large tip-clearances for a two-stage heat pump concept," *International Journal of Refrigeration*, vol. 69, pp. 285–302, 2016, ISSN: 0140-7007. DOI: https://doi.org/10.1016/j.ijrefrig.2016.06.015. [Online]. Available: https://www.sciencedirect.com/science/article/pii/S0140700716301773.

[9] Eckert, T., Dostal, L., Helm, M., and Schweigler, C., "3d-cfd design study and optimization of a centrifugal turbo compressor for the operation in a hybrid sorption/ compression heat pump cycle," 2016.

[10] Wang, Y., Lin, F., Nie, C., and Engeda, A., "Design and performance evaluation of a very low flow coefficient centrifugal compressor," *International Journal of Rotating Machinery*, vol. 2013, Sep. 2013. DOI: 10.1155/2013/293486.

[11] Grassi, W., *Heat Pumps: Fundamentals and Applications*, eng, ser. Green Energy and Technology. Cham: Springer International Publishing AG, 2017, ISBN: 331962198X.

[12] Arpagaus, C., Bless, F., Schiffmann, J., and Bertsch, S. S., "Multi-temperature heat pumps: A literature review," *International Journal of Refrigeration*, vol. 69, pp. 437–465, 2016, ISSN: 0140-7007. DOI: https://doi.org/10.1016/j.ijrefrig.2016.05.014. [Online]. Available: https://www.sciencedirect.com/science/article/pii/S0140700716301190.

[13] *Final report for hpt tcp annex 47 – "heat pumps in district heating and cooling systems"*, https://heatpumpingtechnologies.org/annex47/final-report-for-hpt-tcp-annex-47-heat-pumps-in-district-heating-and-cooling-systems/.

[14] Chua, K., Chou, S., and Yang, W., "Advances in heat pump systems: A review," *Applied Energy*, vol. 87, no. 12, pp. 3611–3624, 2010, ISSN: 0306-2619. DOI: https://doi.org/10.1016/j.apenergy.2010.06.014. [Online]. Available: https://www.sciencedirect.com/science/article/pii/S030626191000228X.

[15] Zhang, J., Zhang, H.-H., He, Y.-L., and Tao, W.-Q., "A comprehensive review on advances and applications of industrial heat pumps based on the practices in china," *Applied Energy*, vol. 178, pp. 800–825, 2016, ISSN: 0306-2619. DOI: https://doi.org/10.1016/j.apenergy.2016.06.049. [Online]. Available: https://www.sciencedirect.com/science/article/pii/S0306261916308248.

[16] van de Bor, D. and Infante Ferreira, C., "Quick selection of industrial heat pump types including the impact of thermodynamic losses," *Energy*, vol. 53, pp. 312–322, 2013, ISSN: 0360-5442. DOI: https://doi.org/10.1016/j.energy.2013.02.065. [Online]. Available: https://www.sciencedirect.com/science/article/pii/S0360544213002004.

[17] Arpagaus, C., Bless, F., Uhlmann, M., Schiffmann, J., and Bertsch, S. S., "High temperature heat pumps: Market overview, state of the art, research status, refrigerants, and application potentials," *Energy*, vol. 152, pp. 985–1010, 2018, ISSN: 0360-5442. DOI: https://doi.org/10.1016/j.energy.2018.03.166. [Online]. Available: https://www.sciencedirect.com/science/article/pii/S0360544218305759.

[18] Bergland, M. G., *Optimizing the compression/absorption heat pump system at high temperatures*, 2014.

[19] P. Nellissen, S. W., "Heat pumps in non-domestic applications in europe: Potential for an energy revolution," *8th EHPA European Heat Pump Forum*, pp. 1–17, 2015, Cited By :2. [Online]. Available: www.scopus.com.

[20] Grassi, W., *Heat pumps : fundamentals and applications*, ser. Green energy and technology. Springer, 2018, ISBN: 978-3-319-62199-9,3319621998,978-3-319-62198-2. [Online]. Available: http://gen.lib.rus.ec/book/index.php?md5=e77df4e33ccaa9fe5b85615fd51166f0.

[21] Mateu-Royo, C., Arpagaus, C., Mota-Babiloni, A., Navarro-Esbrí, J., and Bertsch, S. S., "Advanced high temperature heat pump configurations using low gwp refrigerants for industrial waste heat recovery: A comprehensive study," *Energy Conversion and Management*, vol. 229, p. 113 752, 2021, ISSN: 0196-8904. DOI: https://doi.org/10.1016/j.enconman.2020.113752. [Online]. Available: https://www.sciencedirect.com/science/article/pii/S0196890420312759.

[22] Bin Hu Di Wu, R. W., "O.3.7.4 performance simulation and exergy analysis on multi-stage compression high temperature heat pumps with r1234ze(z) refrigerant," *12th IEA Heat Pump Conference*, 2017.

[23] Hu, B., Wu, D., Wang, L., and Wang, R., "Exergy analysis of r1234ze(z) as high temperature heat pump working fluid with multi-stage compression," *Frontiers in Energy*, vol. 11, Nov. 2017. DOI: 10.1007/s11708-017-0510-6.

[24] Moisi, H. and Rieberer, R., "Erforderliche sauggasüberhitzung bei einer r600-hochtemperaturwärmepumpe – nutzung der motorabwärme," deutsch, in *Proc. Deutsche Kälte-Klima-Tagung 2016*, Deutsche Kälte-Klima-Tagung ; Conference date: 16-11-2016 Through 18-11-2016, 2016.

[25] Moisi, H. and Rieberer, R., "Refrigerant selection and cycle development for a high temperature vapor compression heat pump," *12th IEA Heat Pump Conference, Rotterdam*, pp. 1–10, 2017, cited By 8.

[26] Hastbacka, M., Dieckmann, J., and Bouza, A., "Centrifugal compressors," *ASHRAE Journal*, vol. 55, no. 2, pp. 63–64, 2013, cited By 2. [Online]. Available: https://www.scopus.com/inward/record.uri?eid=2-s2.0-84875199055&partnerID=40&md5=399c10664cec66da262024a9a5639f06.

[27] Dixon, S. and (Auth.), C. H., *Fluid Mechanics and Thermodynamics of Turbomachinery*, 7th ed. Butterworth-Heinemann, 2014, ISBN: 978-0-12-415954-9. [Online]. Available: http://gen.lib.rus.ec/book/index.php?md5=80f7bf462a749a3d78cd59624570877a.

[28] Marco Gambini, M. V., *Turbomachinery: Fundamentals, Selection and Preliminary Design*, 1st ed., ser. Springer Tracts in Mechanical Engineering. Springer International Publishing;Springer, 2021, ISBN: 978-3-030-51298-9,978-3-030-51299-6. [Online]. Available: http://gen.lib.rus.ec/book/index.php?md5=437b6850e8f3beebfbf20012463bc9b9.

[29] (auth.), D.-I. K. H. L., *Process Centrifugal Compressors: Basics, Function, Operation, Design, Application*, 1st ed. Springer-Verlag Berlin Heidelberg, 2004, ISBN: 978-3-642-07330-4,978-3-662-09449-5. [Online]. Available: http://gen.lib.rus.ec/book/index.php?md5=f40e3acc4dc3c241602976dab65e13dc.

[30] VAN DEN BRAEMBUSSCHE, R., *Design and analysis of centrifugal compressors*. JOHN WILEY, 2020, ISBN: 9781119424093,1119424097. [Online]. Available: http://gen.lib.rus.ec/book/index.php?md5=c767fef8fd2cdb242905df507e4a3535.

[31] *An Evaluation of 1D Design Methods for the Off-Design Performance Prediction of Automotive Turbocharger Compressors*, vol. Volume 8: Turbomachinery, Parts A, B, and C, Turbo Expo: Power for Land, Sea, and Air, Jun. 2012, pp. 915–925. DOI: 10.1115/GT2012-69743. eprint: https://asmedigitalcollection.asme.org/GT/proceedings-pdf/GT2012/44748/915/4233548/915_1.pdf. [Online]. Available: https://doi.org/10.1115/GT2012-69743.

[32] Robinson, C., Casey, M., and Woods, I., "An integrated approach to the aero-mechanical optimisation of turbo compressors," 2011.

[33] Casey, M. and Marty, F., "Centrifugal compressors - performance at design and off-design," *Proceedings of the Institute of Refrigeration, London*, 1965.

[34] Rodgers, C., "Efficiency of centrifugal compressor impellers," *Paper 22 of AGARD conference proceedings No 282 Centrifugal Compressors, Flow Phenomena and Performance, Brussels*, 1980.

[35] Xu, C. and Amano, R., "Empirical design considerations for industrial centrifugal compressors," *International Journal of Rotating Machinery*, vol. 2012, May 2012. DOI: 10.1155/2012/184061.

[36] Wang, Y., Lin, F., Nie, C., and Engeda, A., "Design and performance evaluation of a very low flow coefficient centrifugal compressor," *International Journal of Rotating Machinery*, vol. 2013, Sep. 2013. DOI: 10.1155/2013/293486.

[37] Lüdtke, K. H., *Process Centrifugal Compressors Basics, Function, Operation, Design, Application*, eng, 1st ed. 2004.. 2004, ISBN: 9783642073304.

[38] Šarevski, M. N. and Šarevski, V. N., "Chapter 2 - water (r718) centrifugal compressors," in *Water (R718) Turbo Compressor and Ejector Refrigeration / Heat Pump Technology*, M. N. Šarevski and V. N. Šarevski, Eds., Boston: Butterworth-Heinemann, 2016, pp. 9–60, ISBN: 978-0-08-100733-4. DOI: https://doi.org/10.1016/B978-0-08-100733-4.00002-0. [Online]. Available: https://www.sciencedirect.com/science/article/pii/B9780081007334000020.

[39] Šarevski, M. and Šarevski, V., "Characteristics of water vapor turbocompressors applied in refrigeration and heat pump systems," *International Journal of Refrigeration*, vol. 35, no. 5, pp. 1484–1496, 2012, ISSN: 0140-7007. DOI: https://doi.org/10.1016/j.ijrefrig.2012.03.014. [Online]. Available: https://www.sciencedirect.com/science/article/pii/S0140700712000722.

[40] Arunachalam, V., Nagpurwala, Q. H., Deshpande, M. D., Shankapal, S. R., and Ramaiah, M., "Numerical studies on the effect of impeller blade skew on centrifugal compressor performance," 2008.

[41] Drozdov, A and Galerkin, Y, "The numerical study of the rake angle of impeller blade in centrifugal compressor," *IOP Conference Series: Materials Science and Engineering*, vol. 232, p. 012 036, 2017. DOI: 10.1088/1757-899x/232/1/012036. [Online]. Available: https://doi.org/10.1088/1757-899x/232/1/012036.

[42] Japikse, *Centrifugal Compressor Design and Performance*. ETI, Wilder, VT, 1976-1996.

[43] Shah, S., Jain, S., Patel, R., and Lakhera, V., "Cfd for centrifugal pumps: A review of the state-of-the-art," *Procedia Engineering*, vol. 51, pp. 715–720, 2013, Chemical, Civil and Mechanical Engineering Tracks of 3rd Nirma University International Conference on Engineering (NUiCONE2012), ISSN: 1877-7058. DOI: https://doi.org/10.1016/j.proeng.2013.01.102. [Online]. Available: https://www.sciencedirect.com/science/article/pii/S1877705813001033.

[44] Dewar, B., Tiainen, J., Jaatinen-Värri, A., Creamer, M., Dotcheva, M., Radulovic, J., and Buick, J., "Cfd modelling of a centrifugal compressor with experimental validation through radial diffuser static pressure measurement," *International Journal of Rotating Machinery*, vol. 2019, pp. 1–12, May 2019. DOI: 10.1155/2019/7415263.

[45] Tamma A., G. M. and Stoffel, B., "Experimental and 3-d numerical analysis of the flow field in turbomachines," 1999, Darmstadt.

[46] Rautaheimo P., S. E. and Siikonen, T., "Numerical simulation of the flow in the nasa low-speed centrifugal compressor," no. ISBN 951–22–4360–1, Helsinki University of Technology, Laboratory of Applied Thermodynamics, 1998.

[47] Hanjalić, K. and Launder, B. E., "A reynolds stress model of turbulence and its application to thin shear flows," *Journal of Fluid Mechanics*, vol. 52, no. 4, pp. 609–638, 1972. DOI: 10.1017/S002211207200268X.

[48] Wilcox, D. C., "Formulation of the k-w turbulence model revisited," *AIAA Journal*, vol. 46, no. 11, pp. 2823–2838, 2008. DOI: 10.2514/1.36541. eprint: https://doi.org/10.2514/1.36541. [Online]. Available: https://doi.org/10.2514/1.36541.

[49] Rinaldi, E., Pecnik, R., and Colonna, P., "Steady state cfd investigation of a radial compressor operating with supercritical co2," vol. 8, Jun. 2013, V008T34A008–V008T34A008. DOI: 10.1115/GT2013-94580.

[50] Ameli, A., Turunen-Saaresti, T., and Backman, J., "Numerical Investigation of the Flow Behavior Inside a Supercritical CO2 Centrifugal Compressor," *Journal of Engineering for Gas Turbines and Power*, vol. 140, no. 12, Aug. 2018, ISSN: 0742-4795. DOI: 10.1115/1.4040577.

[51] Bell, I. H., Wronski, J., Quoilin, S., and Lemort, V., "Pure and pseudo-pure fluid thermophysical property evaluation and the open-source thermophysical property library coolprop," *Industrial & Engineering Chemistry Research*, vol. 53, no. 6, pp. 2498–2508, 2014, PMID: 24623957. DOI: 10.1021/ie4033999. eprint: https://doi.org/10.1021/ie4033999. [Online]. Available: https://doi.org/10.1021/ie4033999.

[52] Lemmon EW Huber ML, M. M., "Nist reference fluid thermodynamic and transport properties–refprop," vol. 2002, Sep. 2013.

[53] f-Chart Software, *Ees - engineering equation solver*, version 10.8.3.4. [Online]. Available: http://www.fchart.com/ees/pro-comm-versions.php.

[54] The Mathworks Inc. MATLAB, *Ees - engineering equation solver*. [Online]. Available: http://www.mathwork.com/products/matlab/.

[55] Van Rossum, G. and Drake Jr, F. L., *Python reference manual*. Centrum voor Wiskunde en Informatica Amsterdam, 1995.

[56] Aungier, R. H., *Centrifugal Compressors: A Strategy for Aerodynamic Design and Analysis*. ASME Press, Jan. 2000. [Online]. Available: https://doi.org/10.1115/1.800938.

[57] Li, J., Yin, Y., Li, S., and Zhang, J., "Numerical simulation investigation on centrifugal compressor performance of turbocharger," *Journal of Mechanical Science and Technology*, vol. 27, no. 6, pp. 1597–1601, 2013, ISSN: 1738-494X. DOI: 10.1007/s12206-013-0405-3.

[58] ANSYS, I., *Ansys cfx-pre user's guide*. [Online]. Available: http://www.ansys.com.

[59] Meggers, F., Mast, M., and Leibundgut, H., “The missing link for low exergy buildings: Low temperature-lift, ultra-high cop heat pumps,” Jan. 2010.

[60] Boyce, M. P., “Principles of operation and performance estimation of centrifugal compressors.,” 1993.

[61] MEHRA, A., “Aerodynamic design considerations for the turbomachinery of a micro gas turbine engine,” *The 25th National and 1st International on Fluid Mechanics and Fluid Power, 1998*, 1998. [Online]. Available: `https://ci.nii.ac.jp/naid/10017628036/en/`.

Appendix - Contents

A Thermodynamic cycle MatLab code **50**
A.1 Main File 50
A.2 Function 51

B Second Appendix **56**

Appendix A

Thermodynamic cycle MatLab code

A.1 Main File

```
clear all
close all
clc

Ref='R1234ze(E)';
eta_is_c_1st_stage = 0.85;                  % compressor efficiency [-]
eta_is_c_2nd_stage = 0.85;                  % compressor efficiency [-]
mass_flow_TOT = 95;                         % mass flow [kg/s]
T_cond = 100 + 273;                         % condesnig temperature in [K]
T_control = 75 + 273;                       % returning temperature [K]
Delta_T_SH_1 = 5;                           % Temperature difference
    between T1' and super-heating temperature T1
Delta_T_SH_2 = 5;                           % Temperature difference
    between T8 and super-heating temperature T3
T_evap = -5 +273;
T_cond = 100 +273;



[T_vect, h_vect, P_vect, PI_c_1st_stage_max_COP, PI_c_2nd_stage_max_COP,
    mass_flow_1st_stage_vect_max_COP] = Find_Opt_Pi(Ref,T_evap,T_cond,
    eta_is_c_1st_stage,eta_is_c_2nd_stage,mass_flow_TOT,Delta_T_SH_1)


[gamma_av1, mu_av1, T_crit1, P_crit1, rho_crit1, vol_crit1, AC_fact1] =
    FindGasProperties(Ref,T_vect(1),T_vect(2),P_vect(1),P_vect(2),
    eta_is_c_1st_stage)
[gamma_av2, mu_av2, T_crit2, P_crit2, rho_crit2, vol_crit2, AC_fact2] =
    FindGasProperties(Ref,T_vect(3),T_vect(4),P_vect(3),P_vect(4),
    eta_is_c_2nd_stage)
```

A.2 Function

```
function [T_vect_PI_opt, h_vect_PI_opt, P_vect_PI_opt,
   PI_c_1st_stage_max_COP, PI_c_2nd_stage_max_COP,
   mass_flow_1st_stage_vect_max_COP] = Find_Opt_Pi(Ref,T_evap,T_cond,
   eta_is_c_1st_stage,eta_is_c_2nd_stage,mass_flow_TOT,Delta_T_SH_1)

PI_c_1st_stage_min = 3.8;
PI_c_1st_stage_max = 7;
mass_flow_2nd_stage = mass_flow_TOT;
Delta_T_SC = 20;

R=strcat(Ref);
COP_vect=[];
Comp_Work_1st_st_vect = [];
Comp_Work_2nd_st_vect = [];
Comp_Work_TOT_vect = [];
PI_c_1st_stage_vect = [];
PI_c_2nd_stage_vect = [];
PI_c_1st_stage_OPT_Ref = [];
COP_PI_c_1st_stage_OPT_Ref = [];
it = 0;
Delta_h12 = 1;
PI_c_1st_stage = PI_c_1st_stage_min;
i=0;
mass_flow_1st_stage_vect=[];

while (Delta_h12 >=0)  %&& (PI_c_1st_stage<PI_c_1st_stage_max)

    for  PI_c_1st_stage = [PI_c_1st_stage_min:0.1:PI_c_1st_stage_max]
        i=i+1;


        %PI_c_1st_stage_vect=[PI_c_1st_stage_vect PI_c_1st_stage];

        T_critical= py.CoolProp.CoolProp.PropsSI("Tcrit",R);              %
    Critical Temperature of the refrigerant [K]
        P_critical= py.CoolProp.CoolProp.PropsSI("Pcrit",R) ;             %
    Critical Pressure of the refrigerant [Pa]
        T_cond_max= T_critical;                                           %
    maximum admissible temperature in the condenser [K]

        if (T_cond_max-T_cond)< 10
            %T_cond=T_cond_max;
            fprintf(['The difference between the critical and condensing
   temperature for ',Ref,'is less then 10 K'])
        end

        P_evap = py.CoolProp.CoolProp.PropsSI('P','T',T_evap,'Q',1,R);    %
```

```
 evaporator pressure [Pa]
41      P_cond = py.CoolProp.CoolProp.PropsSI('P','T',T_cond,'Q',0,R);    %
 condenser pressure [Pa]
42      PI_c_tot = P_cond/P_evap;
43
44
45      % STATION 1 (COMPRESSOR: 1st STAGE INLET)
46      P1=P_evap;
47      T1_prime = py.CoolProp.CoolProp.PropsSI('T','P',P1,'Q',1,R);
48      T1= T1_prime + Delta_T_SH_1;
% Temperature at point 1 after super-heating
49      h1 = py.CoolProp.CoolProp.PropsSI('H','P',P1,'T',T1,R);
% enthalpy at station 1 [J/kg]
50      s1 = py.CoolProp.CoolProp.PropsSI('S','P',P1,'H',h1,R);
51      %rho1=  py.CoolProp.CoolProp.PropsSI('D','T',T1,'Q',1,R);
52      rho1=  py.CoolProp.CoolProp.PropsSI('D','P',P1,'T',T1,R);
53      Cp_1 = py.CoolProp.CoolProp.PropsSI('CPMASS','P',P1,'T',T1,Ref);
54
55      % STATION 2 (COMPRESSOR: 1st STAGE OUTLET)
56      s2s = s1;
57      P2= P1*PI_c_1st_stage;
58      h2s = py.CoolProp.CoolProp.PropsSI('H','P',P2,'S',s2s,R);
59      h2 = h1 + (h2s - h1)/eta_is_c_1st_stage;
60      T2 = py.CoolProp.CoolProp.PropsSI('T','P',P2,'H',h2,R);
 % discharge temperature of the 1st stage
61      rho2=  py.CoolProp.CoolProp.PropsSI('D','P',P2,'T',T2,R);
62      Cp_2 = py.CoolProp.CoolProp.PropsSI('CPMASS','P',P2,'T',T2,Ref);
63
64      % CHECK ON DRY COMPRESSION
65      for P12 = P1+ (P2 -P1)*[0:0.05:1];
66             if Delta_h12 <= 0
67                  break
68             else
69                 h12 = h2 - (h2-h1)*(P2-P12)/(P2-P1);
70                 h12_sat = py.CoolProp.CoolProp.PropsSI('H','P',P12,'Q
',1,R);
71                 Delta_h12 = h12 - h12_sat;
72             end
73      end
74
75      % STATION 3 (COMPRESSOR: 2nd STAGE INLET)
76      P3 = P2;
77      T3_prime = py.CoolProp.CoolProp.PropsSI('T','P',P2,'Q',1,R);
  % Temperature at evaporation point
78      T3_old = (T2 + T3_prime)/2;
  % First guess of T3
79      it =0;
80      Delta_T3 = 1;
```

```
81
82          while Delta_T3>1e-3
83              T3 = T3_old;
84              h3 = py.CoolProp.CoolProp.PropsSI('H','P',P3,'T',T3,R);
85              s3 = py.CoolProp.CoolProp.PropsSI('S','P',P3,'T',T3,R);
86
87              % STATION 4 (COMPRESSOR: 2nd STAGE OUTLET)
88              s4s = s3;
89              P4 = P_cond;
90              h4s = py.CoolProp.CoolProp.PropsSI('H','P',P4,'S',s4s,R);
91              h4 = h3 + (h4s - h3)/eta_is_c_2nd_stage;
92              T4 = py.CoolProp.CoolProp.PropsSI('T','P',P4,'H',h4,R);
     % discharge temperature of the 2nd stage
93              PI_c_2nd_stage = P4/P3;
94
95
96              % STATION 5
97              P5 = P4;
98              T5 = py.CoolProp.CoolProp.PropsSI('T','P',P5,'Q',0,R);
99              h5 = py.CoolProp.CoolProp.PropsSI('H','P',P5,'Q',0,R);
100
101             % STATION 6
102             P6 = P5;
103             T6 = T5 - Delta_T_SC;
104             %T6 = T_control;
105             h6 = py.CoolProp.CoolProp.PropsSI('H','P',P6,'T',T6,R);
106
107
108             % STATION 7
109             h7 = h6;
110             P7 = P3;
111             X7 = py.CoolProp.CoolProp.PropsSI('Q','H',h7,'P',P7,R);
112             T7 = py.CoolProp.CoolProp.PropsSI('T','P',P7,'Q',X7,R);
113             mass_flow_1st_stage = mass_flow_TOT*(1-X7);
114             mass_flow_intermediate = mass_flow_TOT - mass_flow_1st_stage;
115
116             T3 = (mass_flow_1st_stage*T2 + T3_prime*mass_flow_intermediate)
    / mass_flow_TOT;
117             Delta_T3 = abs(T3 - T3_old);
118             T3_old = T3;
119             it = it+1;
120         end
121
122         % STATION 8
123         P8 = P7;
124         T8 = py.CoolProp.CoolProp.PropsSI('T','P',P8,'Q',1,R);
125         h8 = py.CoolProp.CoolProp.PropsSI('H','P',P8,'Q',1,R);
126
```

```
127
128         % STATION 9
129         P9 = P8;
130         T9 = py.CoolProp.CoolProp.PropsSI('T','P',P9,'Q',0,R);
131         h9 = py.CoolProp.CoolProp.PropsSI('H','P',P9,'Q',0,R);
132
133         % STATION 10
134         h10 = h9;
135         P10 = P1;
136         T10 = py.CoolProp.CoolProp.PropsSI('T','P',P10,'H',h10,R);
137
138         T_vect = [T1 T2 T3 T4 T5 T6 T7 T8 T9 T10];                      %
    final Temperature values [K]
139         h_vect = [h1 h2 h3 h4 h5 h6 h7 h8 h9 h10]*1e-3;                 %
    final Enthalpies values [kJ/kg]
140         P_vect = [P1 P2 P3 P4 P5 P6 P7 P8 P9 P10];                      %
    final pressure values [Pa]
141         P_dome_left = [P10:1e3:P_critical*0.95];
142         P_dome_right = [P1:1e3:P_critical*0.95];
143         mass_flow_1st_stage_vect = [mass_flow_1st_stage_vect
    mass_flow_1st_stage];
144
145         COP = mass_flow_2nd_stage*(h_vect(4)-h_vect(6))/(
    mass_flow_1st_stage*(h_vect(2)-h_vect(1))+mass_flow_2nd_stage*(h_vect(4)
    -h_vect(3)));
146         COP_vect=[COP_vect COP];
147         Compressor_Work_1st_stage = mass_flow_1st_stage*(h_vect(2)-h_vect
    (1)); % work of the compressor's 1st stage
148         Compressor_Work_2nd_stage = mass_flow_2nd_stage*(h_vect(4)-h_vect
    (3)); % work of the compressor's 2nd stage
149         Compressor_Work_TOT = Compressor_Work_1st_stage +
    Compressor_Work_2nd_stage;
150
151         Comp_Work_1st_st_vect = [Comp_Work_1st_st_vect
    Compressor_Work_1st_stage];
152         Comp_Work_2nd_st_vect = [Comp_Work_2nd_st_vect
    Compressor_Work_2nd_stage];
153         Comp_Work_TOT_vect = [Comp_Work_TOT_vect Compressor_Work_TOT];
154
155         PI_c_1st_stage_vect = [PI_c_1st_stage_vect PI_c_1st_stage];
156         PI_c_2nd_stage_vect = [PI_c_2nd_stage_vect PI_c_2nd_stage];
157
158
159         T_vect_PI{i} = T_vect;
160         h_vect_PI{i} = h_vect;
161         P_vect_PI{i} = P_vect;
162     end
163
```

```
end

[COP_max,k] = max(COP_vect);
PI_c_1st_stage_max_COP = PI_c_1st_stage_vect(k);
PI_c_2nd_stage_max_COP = PI_c_2nd_stage_vect(k);
mass_flow_1st_stage_vect_max_COP = mass_flow_1st_stage_vect(k);

T_vect_PI_opt = T_vect_PI{k};
h_vect_PI_opt = h_vect_PI{k};
P_vect_PI_opt = P_vect_PI{k};


h_dome_left=[];
h_dome_right=[];
for P=P_dome_left
    h = py.CoolProp.CoolProp.PropsSI('H','P',P,'Q',0,R);
    h_dome_left = [h_dome_left h*1e-3];
end


for P=P_dome_right
    h = py.CoolProp.CoolProp.PropsSI('H','P',P,'Q',1,R);
    h_dome_right = [h_dome_right h*1e-3];
end

figure
plot([ h_vect_PI{k}(1:7)  h_vect_PI{k}(9:10)  h_vect_PI{k}(1)], [ P_vect_PI
    {k}(1:7)  P_vect_PI{k}(9:10)  P_vect_PI{k}(1)],'o-','LineWidth',2)
hold on
plot([h_vect_PI{k}(7) h_vect_PI{k}(3)],  [P_vect_PI{k}(7)  P_vect_PI{k}(8)
    ],'Color','[0 0.4470 0.7410]','LineStyle','--','LineWidth',2)
plot(h_dome_right, P_dome_right,'r')
plot(h_dome_left, P_dome_left,'r')
title(['P-h diagram: ', R,' @ \Pi_c^{opt}'])
ylabel('Pressure [Pa]')
xlabel('Enthalpy [kJ/kg]')
ylim([0 1.2*P_vect(5)])

figure
plot(PI_c_1st_stage_vect, COP_vect,'LineWidth',2)
hold on
plot(PI_c_1st_stage_max_COP,COP_max,'r*','LineWidth',2)
title('COP VS \Pi_c 1^{st} stage')
ylabel('COP [-]')
xlabel('1^{st} stage pressure ratio [-]')
legend(Ref,'Location','northeast')
grid on
```

Appendix B

Second Appendix

this is the information